Multi-proxy evidence for millennial-scale changes in North Pacific Holocene hydroclimate from the Kenai Peninsula lowlands, south-central Alaska

Ellie Broadman[1*], Darrell S. Kaufman[1], Andrew C. G. Henderson[2], Edward E. Berg[3], R. Scott Anderson[1], Melanie J. Leng[4,5], Sean A. Stahnke[1], Samuel E. Muñoz[6]

[1]School of Earth and Sustainability, Northern Arizona University, Flagstaff, Arizona, USA

[2]School of Geography, Politics & Sociology, Newcastle University, Newcastle upon Tyne, UK

[3]Kenai National Wildlife Refuge, U.S. Fish and Wildlife Service, Soldotna, Alaska, USA

[4]National Environmental Isotope Facility, Isotope Geosciences Facility, British Geological Survey, Keyworth, Nottingham, UK

[5]Centre for Environmental Geochemistry, School of Biosciences, University of Nottingham, Nottingham, UK

[6]Marine Science Center, Department of Marine & Environmental Science, Northeastern University, Nahant, Massachusetts, USA

*** Correspondence:**

Ellie Broadman

ebb42@nau.edu

Keywords: diatom oxygen isotopes, biogenic silica, Kenai lowlands, Aleutian Low, hydroclimate, south-central Alaska, Holocene

Abstract

The Holocene hydroclimate of south-central Alaska has been studied extensively, but conflicting interpretations between oxygen isotope paleoclimate datasets are seemingly as common as converging reconstructions, in part due to the challenges of interpreting oxygen isotope ratios in terms of climate. Here, we present a new Holocene record of biogenic silica abundance (BSi), diatom flora, and diatom oxygen isotopes ($\delta^{18}O_{BSi}$) analyzed in sediments from Sunken Island Lake (SIL) in the Kenai Peninsula lowlands, which we interpret in the context of previously published paleoclimate records, and use to understand regional changes in hydroclimate. Changes in lake level documented by aerial photography coupled with a survey of regional lake water isotopes indicate SIL is sensitive to changes in the balance of precipitation and evaporation (P-E). However, an analysis of SIL $\delta^{18}O_{BSi}$ over the instrumental period indicates that $\delta^{18}O_{BSi}$ is sensitive to both P-E and the isotope composition of precipitation ($\delta^{18}O_{precip}$), which is driven by changes in the Aleutian Low atmospheric pressure cell (AL). We attribute a ~2‰ increase in $\delta^{18}O_{BSi}$ from 5.5 – 4.5 ka cal BP to a stronger AL, which resulted in the delivery of isotopically heavier precipitation to the Kenai lowlands, and wetter conditions during the late Holocene. These interpretations are supported by late Holocene increases in the relative abundance of planktonic diatoms and BSi-inferred storminess, and by evidence for higher-than-present lake levels on the paleo-shorelines above SIL at ~1.5 – 0.5 ka cal BP. Our dataset demonstrates that this region was characterized by relatively low lake levels and dry climate in the early Holocene, a strengthening of the AL in the late Holocene, and wetter climate during the late Holocene until recent decades.

1 Introduction

The hydroclimate of the northeastern Pacific continental margin is of interest to both modern and paleo-climatologists due to the importance of the synoptic-scale ocean-atmospheric dynamics that influence the region. The terrestrial hydroclimate of southeastern Beringia is particularly sensitive to these dynamics, in part due to the pronounced influence of changes in the position and intensity of the Aleutian Low (AL), an atmospheric low pressure cell that affects the strength and trajectory of winter storms (Rodionov et al., 2007). AL variability can therefore cause increased or decreased winter season precipitation, as well as changes to the oxygen isotope composition of precipitation ($\delta^{18}O_{precip}$), which result from different source waters and storm trajectories. These changes in

$\delta^{18}O_{precip}$ are often inferred from proxy data in paleoclimate archives and used to reconstruct AL variability. Comparisons between $\delta^{18}O$ records and the North Pacific Index (NPI – an index of area-weighted sea level pressure over the North Pacific), which is strongly inversely related to the strength of the AL (Trenberth and Hurrell, 1994), are often used to confirm the relationship between $\delta^{18}O$ and the AL (e.g. Bailey et al., 2015). In recent decades, many studies on the Holocene hydroclimate of southern Alaska and southwestern Yukon have used fluctuations in $\delta^{18}O$ to reconstruct changes in the AL, contributing substantially to our knowledge of the pressure cell's Holocene evolution (Anderson et al., 2005; Fisher et al., 2008; Schiff et al., 2009; Jones et al., 2014, 2019; Bailey et al., 2015, 2018). Despite this wealth of literature, our confidence in Holocene AL variability remains limited because of contradictory interpretations of paleo-AL behavior among paleoclimate datasets (e.g. Schiff et al., 2009; Jones et al., 2014; Kaufman et al., 2016) and confounding factors associated with the variety of materials analyzed for $\delta^{18}O$ (bulk organic matter, endogenic calcite, biogenic silica, glacier ice, leaf waxes, and *Pisidium* shells). Additionally, a recent study of $\delta^{18}O_{precip}$ in Anchorage, Alaska revealed that, while $\delta^{18}O_{precip}$ is influenced by synoptic-scale atmospheric circulation patterns related to AL conditions, there is no statistically significant relation between $\delta^{18}O_{precip}$ and the NPI, calling into question the efficacy of using $\delta^{18}O$ records to reconstruct shifts in AL strength and position in this region (Bailey et al., 2019).

While the details of the Holocene history of the AL remain unclear (Kaufman et al., 2016), some features of the hydroclimate of southern Alaska are relatively consistent among existing paleoclimate datasets. For example, Barron and Anderson (2011) identified a shift in terrestrial hydroclimate associated with a strengthened AL at ~4 ka cal BP throughout the northeastern Pacific Rim, which would have increased moisture flow to southern Alaska. This late Holocene hydroclimatic shift has been corroborated by more recent $\delta^{18}O$ reconstructions that also identify a strengthened AL at this time (Jones et al., 2014; Bailey et al., 2018). This inferred AL shift also corresponds roughly to a period characterized by wetter conditions throughout southeastern Beringia in the late Holocene (Kaufman et al., 2016).

To further examine Holocene hydroclimate and related environmental changes in south-central Alaska, we present a new biogenic silica (BSi), diatom flora, and diatom oxygen isotope ($\delta^{18}O_{BSi}$) record from Sunken Island Lake in the Kenai Peninsula lowlands. Diatoms are abundant in the sedimentary record of most non-alkaline lakes and have an unambiguous source of $\delta^{18}O$ from the lake water in which they make their silica-based frustules, a process thought to occur in isotopic equilibrium with lake water (Leng and Barker, 2006). Therefore, $\delta^{18}O_{BSi}$ is a proxy well suited to reconstructing paleoclimate conditions in this region. Our results provide evidence for a late Holocene increase in both effective moisture and southerly-derived precipitation, and highlight the complexity of interpreting paleo-$\delta^{18}O$ data in the dynamic and multi-faceted North Pacific hydroclimate setting.

1.1 Study area

The Kenai Peninsula is located in south-central Alaska, bordered by Cook Inlet and the Gulf of Alaska (GoA) (Fig. 1A). The Kenai Mountains occupy the southeastern portion of the peninsula, and act as a barrier to storms traveling from the GoA, creating a rain shadow effect in the Kenai lowlands to the northwest. Mean annual temperature at the Kenai Moose Pens SNOTEL site was 2.7°C, mean annual rainfall was 47.2 cm, and mean annual snow-water equivalent was 11.4 cm between 1995 and 2019 (National Water and Climate Center, https://www.wcc.nrcs.usda.gov/index.html). The majority of precipitation in the Kenai Peninsula occurs from November to March, when the AL strengthens and moves eastward, as opposed to spring and summer months when it weakens and moves westward (Overland et al., 1999) (Fig. 2). These seasonal changes in the AL also have a strong influence on the average path of winter storms: a strong AL directs storms from the southwest to the GoA and south-central region of the state, whereas a weak AL sends storms west and northwest to travel across Alaska before reaching the same region (Rodionov et al., 2007) (Fig. 3). These seasonal changes in precipitation are accompanied by seasonal changes in temperature and $\delta^{18}O_{precip}$ (Fig. 2). The relative strength and position of the AL also vary interannually, resulting in stormier and less stormy years in south-central Alaska. Both seasonal and interannual shifts in average storm trajectories associated with the AL also influence $\delta^{18}O_{precip}$ (Fig. 3), where interannual fluctuations superimpose an isotope imprint on the average seasonal change.

Sunken Island Lake (SIL; 60.592°, –150.883°; 76 m a.s.l.) is one of many kettles holes that formed in the Kenai lowlands during the recession of the Moosehorn stade of the Naptowne glaciation, which commenced ~23 – 19 ka cal BP following ice advances from both the Alaska Range and the Kenai Mountains (Reger et al., 2007). SIL comprises a large, deep sub-basin in its southern portion (16.8 m maximum water depth), and two smaller sub-basins in the north and east (7.4 m and 7.0 m maximum water depth respectively) (Fig. 1B). The lake is topographically closed, lacking a permanent inflow and outflow, and is therefore primarily fed by precipitation and groundwater. SIL is thermally stratified in the summer months: in June 2017, water surface temperature was 16.2°C, and bottom water temperatures were 10.6°C at 7.0 m water depth in the eastern sub-basin and 6.4°C at 16.8 m water depth in the southern sub-basin. Conductivity of SIL water ranged from 35 to 45 $\mu S\ cm^{-1}$. Aerial photographs show that lake surface elevation was ~78.5 m a.s.l in 1950 CE, and lowered to ~75.5 m a.s.l by 2011 CE, indicating that substantial lake-level fluctuations occur at this site (Fig. 1C-D).

2 Methods

2.1 Regional water sampling and isotope analyses

To determine whether evaporation influences the isotope composition of lake water ($\delta^{18}O_{lake}$) at SIL and to characterize the $\delta^{18}O$ of the components of the local hydrologic system, a water sampling campaign was undertaken in the Kenai lowlands in June 2017, June 2018, and August 2018. Water samples were collected in 125 mL polyethylene bottles from 27 lakes (including SIL), 2 rivers, and a groundwater well (n = 84). Following each field season, water samples were processed using Wavelength-Scanned Cavity Ringdown Spectroscopy at the Colorado Plateau Analytical Laboratory at Northern Arizona University. Analytical precision was ≤ 0.3‰ for $\delta^{18}O$ and ≤ 0.6‰ for δD (1σ).

2.2 Sediment core recovery, sedimentological analyses, and geochronology

Sediment core SIL-04-01 (821 cm long) was taken from the northern sub-basin of SIL (60.5962°, –150.8779°; 7.4 m water depth) (Fig. 1B) in June 2004 using a 5-cm-diameter Livingstone piston corer. Upon recovery, core segments were split, and the sediment stratigraphy described. Magnetic susceptibility (MS) was analyzed at 5 mm spacing using a Bartington MS2E surface probe. Loss on ignition (LOI) was completed for each contiguous 1 cm increment, where each 1 cm^3 sample was weighed and dried overnight in an oven, then re-weighed and burned at 550°C for 2 hours, and finally weighed again to calculate LOI (Dean, 1974). SIL-04-01 has been previously analyzed for pollen, macrofossils, and charcoal (Anderson et al., 2019).

Plant and insect macrofossils from SIL-04-01 provide an existing geochronological framework (Anderson et al., 2019), but the core has been heavily sub-sampled for previous analyses. Additional material was needed for our sediment-intensive diatom oxygen isotope sampling. Therefore, in June 2017 sediment cores were taken from four sites across SIL (Fig. S1) using a percussion piston coring system. Upon recovery, cores were split, described, and analyzed for bulk density and MS using

Geotek MSCL-S and MSCL-XYZ automated core loggers at the National Lacustrine Core Facility (LacCore) at the University of Minnesota, Minneapolis. Sediment cores from the deepest, southern basin of the lake (16.8 m water depth; SIL17-2 and SIL17-3) were not analyzed in this study because the stratigraphy of these sequences indicates they may contain one or more slump deposits (Fig. S1). Of the other two sediment sequences, the core from the eastern sub-basin (SIL17-1; 60.5916°, –150.8854°; 7.0 m water depth; Fig. 1B) was > 1 m longer (401 cm) than the core from the northern basin (SIL17-4). SIL17-1 was therefore used in this study due to the large sample sizes needed for analyzing $\delta^{18}O_{BSi}$. Though SIL17-1 was the longest sediment sequence collected in 2017, it did not capture the entire Holocene record, and therefore the lower portion of SIL-04-01 was still needed to complete the $\delta^{18}O_{BSi}$ dataset. MS measurements and prominent tephra layers were used to provide tie points between cores SIL17-1 and SIL-04-01 in order to establish a geochronology for the upper ~4 m of SIL17-1 using existing ages from SIL-04-01 (Fig. S2). This transfer of previously acquired ages gave rise to a composite ~750 cm "master core" (SIL-MC), which comprises ~4 m of SIL17-1 and the lower ~3.5 m of SIL-04-01 (Supplementary Data). SIL-MC was used for all sampling and original analyses presented in this study. To compare existing analyses from SIL-04-01 (Anderson et al., 2019) to the BSi, diatom assemblage, and $\delta^{18}O_{BSi}$ data, the depths and values from SIL-04-01 were adjusted according to regression relationships derived from the cores' shared tie points from the MS and tephras (Supplementary Data).

Percent biogenic silica by mass (BSi) was determined for SIL-MC using wet-alkaline extraction (10% Na_2CO_3), molybdate-blue reduction, and spectrophotometry (Mortlock and Froelich, 1989). Sampling resolution was every 0.5 cm for the upper 15 cm, and every 8 cm downcore (n = 130). A duplicate was analyzed for every 4 or 5 samples (n = 30) to determine the reproducibility of the procedure. Duplicates were processed in separate batches, and samples in each batch were selected randomly from all sample depths.

^{210}Pb and ^{137}Cs profiles were used to constrain the chronology for the last ~100 years of surface core SIL17-1B (Fig. S3; Table S1). The previously published ^{210}Pb-based chronology from SIL-04-01 (Anderson et al., 2019) was not used because SIL17-1 includes sediments deposited between 2004 and 2017, necessitating a new surface sediment chronology that incorporates these youngest sediments that were analyzed for BSi and $\delta^{18}O_{BSi}$. ^{210}Pb, ^{214}Pb, and ^{137}Cs γ-activities were measured on 14 oven-dried and powdered samples from the upper 19 cm of SIL17-1B using a Canberra Broad Energy Germanium Detector (BEGe; model no. BE3830P-DET), with a count time of 24 hours. The Constant Rate of Supply (CRS) model (Appleby, 2001) was used to estimate ages and confidence intervals of the samples with excess ^{210}Pb activities above equilibrium with ^{214}Pb. Samples were analyzed at the Earth Surface Systems Laboratory at the Marine Science Center at Northeastern University.

The down-core chronology for SIL-MC was established using 16 AMS ^{14}C dates on plant and insect macrofossils from SIL17-1 (n = 1) and SIL-04-01 (n = 15). Ages from SIL-04-01 were "mapped" onto SIL17-1 using least-squares regressions derived from prominent marker layers and MS peaks shared between the sediment sequences (Fig. S2). For all ^{14}C ages, sediment samples 1-2 cm thick were sieved at 150 µm, and macrofossils were then picked, dried in an oven at 50°C, and identified under a Zeiss light microscope. Macrofossils were prepared and converted to graphite at Northern Arizona University, and ^{14}C content was measured at the Keck-Carbon Cycle AMS facility at UC Irvine.

Uncalibrated ^{14}C dates and the ages from the ^{210}Pb model output were incorporated into an age model for the entire sediment sequence using the R package Bacon (v2.2) (Blaauw and Christen, 2011), which calibrates ^{14}C years to calendar years using IntCal13 (Reimer et al., 2013). Chronological uncertainties for the BSi and $\delta^{18}O_{BSi}$ time series were generated in GeoChronR (McKay et al., 2018) using the ensemble output from the Bacon age model.

To constrain fluctuations in Holocene lake level, sediments from satellite fens and ice-shoved ramparts surrounding SIL were acquired and dated. Cores were collected from five satellite fens near SIL using a 2.5-cm-diameter piston corer designed to capture the lowermost 45 cm of peat above mineral soil. AMS ^{14}C dates were determined for macrofossils in the lowermost peat horizons. A prominent 1400-m long ice-shoved rampart was also excavated at two sites. Thrust events in soil profiles in the ice-shoved rampart were identified, and AMS ^{14}C dating was completed on macrofossils below the thrust events in order to chronologically constrain the thrust event.

2.3 Diatom assemblage analysis

Twenty 1-cm-thick samples from SIL-MC were selected at 30-50 cm increments for diatom species analysis. These samples were treated with 30% H_2O_2 and 70% HNO_3 to remove organic matter before creating slides for counting using Naphrax© mounting medium. A Zeiss light microscope was used to count three hundred valves per slide along transects at 1000X magnification, and taxonomic identifications were made according to Foged (1971), Foged (1981), Krammer and Lange-Bertalot (1986-1991), Mann et al. (2004), and McGlaughlin and Stone (1986). Diatom nomenclature was updated following Spaulding et al. (2019). Following identification, diatom species counts were converted to percent relative abundance and graphed with Tilia (v.2.1.1) (Grimm, 2015). An incremental sum-of-squares cluster analysis (CONISS) was applied to dominant taxa with a relative abundance > 5% in at least one sample (Grimm, 1987) to determine zones in the sequence. A principal component analysis (PCA) (ter Braak and Prentice, 1988) was completed on the correlation matrix of untransformed percentage data for all dominant taxa.

2.4 Diatom oxygen isotope analysis

Samples for diatom oxygen isotope analysis (1 cm thick) were taken from SIL-MC every ~10 cm downcore, and every 1 cm of the upper 20 cm (n = 106). Because the oldest sediments were taken from heavily-sampled SIL-04-01, sampling intervals are less consistent over the deepest ~3.5 m of SIL-MC. Sampling avoided visible tephra layers. Samples were purified using a series of chemical digestions, sieving, and heavy liquid separations (*cf.* Morley et al., 2004). All samples were visually inspected for contamination under a Zeiss light microscope, and 30 samples were inspected further using a Zeiss Supra 40VP variable pressure field emission scanning electron microscope (SEM) (e.g. Fig. 4) and energy dispersive X-ray spectroscopy (EDS). $\delta^{18}O_{BSi}$ values were measured by using the stepwise fluorination method (Leng and Sloane, 2008) in the stable isotope facility at the British Geological Survey in Keyworth, UK. $\delta^{18}O$ are reported as per mil (‰) deviations of the isotopic ratio ($^{18}O/^{16}O$) calculated to the VSMOW scale using a within-run laboratory standard calibrated against NBS-28. The measured $\delta^{18}O$ of the standard silica (BFC) was 28.9‰ (n = 16) with an analytical reproducibility of 0.2‰. Analytical reproducibility of the sample material was < 0.3‰ for $\delta^{18}O$ (1σ).

3 Results

3.1 Regional water isotopes

Water isotope values from the 75 lake water samples (Table S2) have a $\delta^{18}O$ range of 8.3‰ (–15.1 to –6.8‰ VSMOW) and a δD range of 38.9‰ (–121.9 to –83.0‰ VSMOW), yielding a Local Evaporation Line (LEL) with a slope of 4.65 (Fig. 5). Water from SIL plots on the far right of the LEL ($\delta^{18}O$ range: –9.3 to –8.4‰ VSMOW; δD range: –94.0 to –87.5‰ VSMOW; Fig. 5). $\delta^{18}O$ and δD values are lower for samples from groundwater and the Kenai and Moose Rivers, some of which are situated close to the Global Meteoric Water Line (GMWL).

3.2 Sediment stratigraphy and geochronology

The ^{210}Pb activities exhibit a gradual decline over the upper 11 cm of core SIL17-1B towards an equilibrium of ~8.3 Bq/kg (Fig. 6; Fig. S3; Table S1). Four samples were excluded from the CRS calculations because they contain low levels of excess ^{210}Pb, likely due to the presence of old material reintroduced to the lake bottom. The ^{137}Cs activities were not used as an independent chronological control because ^{137}Cs activities were generally low, and the peak is poorly defined. The offset between the ^{137}Cs peak and the ^{210}Pb-inferred age model (Fig. 6), as well as low excess ^{210}Pb in the 4 samples described above, might be due to slumping associated with the Prince William Sound earthquake of 1964 CE, which has been previously linked to turbidite deposits (Praet et al., 2017; Boes et al., 2018) and subsidence (Hamilton and Shennan, 2005) in the Kenai lowlands. The sedimentation rate since 1950 CE inferred from the ^{210}Pb model (~1.2 mm/year) is comparable to that reported by Anderson et al. (2019) (~1.3 mm/year).

The oldest reliable age in the SIL age-depth model is from 705.5 cm and is calibrated to 12261 ± 280 a BP (Fig. 6; Table 1). Two older ages were included in the age-depth model, but they are stratigraphically reversed and imply an exceedingly low sedimentation rate, or an unconformity. This implies the age model is not reliable in the inorganic mud below 705.5 cm depth, but diatoms are essentially absent in these sediments (BSi ≤ 1.3% below 712 cm) so this has no influence on our BSi- and isotope-based conclusions. Three ^{14}C ages between 8 – 6 ka cal BP were excluded from the age model, all of which were small macrofossil samples (0.03 – 0.06 mg graphitized carbon) with relatively high analytical uncertainties (214 – 563 years). The ~770 cm sediment sequence captures at least the entire Holocene and the late Younger Dryas, with average 95% confidence intervals of ± 312 years (min = 1; max = 1268 years).

SIL sediments are composed primarily of gyttja, with 26 visible tephras (≥ 1 mm thick) that correspond to pronounced peaks in MS (Fig. 7; Table S3). The basal ~50 cm is interbedded, gray, inorganic clays, silts, and sands likely sourced from sediments associated with the unstable, recently deglaciated landscape that dominated the Kenai lowlands after ~19 ka cal BP (Reger et al., 2007). Organic matter content, as measured by LOI, fluctuates between 20 – 30% throughout the sediments above the basal inorganic unit (Anderson et al., 2019). BSi ranges from 0.2 – 24.2% over the

Holocene (mean = 9.8%), with the increase in BSi content starting in the early Holocene and peaking at its highest values in the mid Holocene between ~6.3 – 4.6 ka cal BP, and decreasing thereafter (Supplementary Data). Analytical reproducibility as indicated by differences between duplicate samples averages 0.97 ± 0.86% (1σ) across the core.

3.3 Diatom assemblages

The diatom assemblages from SIL are diverse, composed of 141 identified taxa, from which 15 dominant species were identified. Dominant species were grouped into one of three habitat types as specified by Spaulding et al. (2019): planktonic diatoms, which are non-motile and occupy the water column; facultatively planktonic diatoms, which may be motile, often dwelling in the lake's benthos, but can elect to live in the water column when it is ecologically advantageous; and benthic diatoms, which can be motile, or live attached to substrates on the lake floor or in shallow sediments. Dominant genera at SIL include planktonic (*Aulacoseira*, *Discostella*), facultatively planktonic (*Pseudostaurosira*, *Staurosira*, *Staurosirella*), and benthic (*Nitzschia*, *Pinnularia*, *Planothidium, Sellaphora*) diatoms. Based on the CONISS dendrogram, changes in the relative abundances of these taxa were divided into four zones (Fig. 8).

Zone 1 (12 – 8.5 ka cal BP; 695 – 570 cm) is characterized by a high abundance of *Staurosirella pinnata*, and the highest recorded abundances of *Discostella stelligera*, *Pinnularia saprophila, Nitzschia palea*, *Sellaphora disjuncta*, and *Sellaphora saugerresii*. Approaching 9 ka cal BP, other benthic taxa increase in abundance as the three dominant species in the zone diminish.

Zone 2 (8.5 – 4.6 ka cal BP; 570 – 300 cm) is dominated by facultatively planktonic taxa such as *S. pinnata*, *Staurosirella leptostauron* var. *dubia*, *Pseudostaurosira brevistriata*, *Pseudostaurosira pseudoconstruens*, and *Pseudostaurosira parasitica*. At ~6 ka cal BP there is an increase in the relative abundance of planktonic taxa such as *Aulacoseira subarctica*, *Aulacoseira valida*, and *D.*

stelligera, which then diminish. *Planothidium joursacense* becomes the dominant benthic species in this zone.

Zone 3 (4.6 – 1 ka cal BP; 300 – 80 cm) features an increase in planktonic species, particularly *A. valida* and *D. stelligera*. Relatively high abundances of *S. pinnata* are present throughout this zone, but facultatively planktonic taxa generally become less abundant with time. *Planothidium frequentissimum* and *P. joursacense* are the dominant benthic taxa in this zone.

Zone 4 (1 ka cal BP – present; 80 – 0 cm) is dominated by the highest recorded abundances of the facultatively planktonic species *Staurosira construens* and *S. pinnata*, and by a decrease in the relative abundance of both planktonic and benthic taxa.

The first two principle components (PCs) of the stratigraphic diatom assemblage data account for 65.4% of the overall variance in the record (λ_1 = 0.419; λ_2 = 0.235), and largely track changes in *S. pinnata* (λ_1) and the opposing relation between *D. stelligera* and several fragilarioid species including *S. construens*, *P. brevistriata*, and *P. parasitica* (λ_2) (Fig. 9).

3.4 Diatom oxygen isotopes

The $\delta^{18}O_{BSi}$ data show a Holocene range of 5.7‰ (+26.5 to +32.2‰ VSMOW, *n* = 98) with a mean of +29.2 ‰ (*n* = 55) prior to 4.5 ka cal BP, which shifts to a mean of +30.7‰ (*n* = 24) between 4.5 and ~1 ka cal BP, followed by a decrease in the mean to +28.3‰ (*n* = 27) over the past ~1 ka cal BP (Fig. 7; Supplementary Data). SEM images indicate that contamination by clay minerals and tephras is insignificant (e.g. Fig. 4). EDS data reveal that the percent of Al_2O_3, commonly used as an indicator of clay contamination in purified biogenic silica (Brewer et al., 2008), is < 1% in all samples. Because sedimentary diatom frustules may contain up to 1% Al_2O_3 incorporated into the silica matrix (Koning et al., 2007), this result further indicates that samples analyzed for $\delta^{18}O_{BSi}$ comprise pure biogenic silica.

4 Discussion

4.1 Climate controls on proxy datasets

To determine controls on $\delta^{18}O_{BSi}$ and BSi in SIL, the data covering the instrumental period were analyzed for their statistical relations with climate variables of interest. Daily precipitation data collected at Kenai airport (http://climate.gi.alaska.edu/acis_data) were summed into annual totals, and then re-sampled to average over the intervals of the $\delta^{18}O_{BSi}$ and BSi sediment samples from SIL using the software package Analyseries (Paillard et al., 1996). Significance calculations were adjusted to correct for auto-correlated time series using a lag-one autocorrelation model (Bretherton et al., 1998) prior to calculating correlation coefficients. Additionally, to relate the $\delta^{18}O_{BSi}$ data to North Pacific ocean-atmosphere circulation, the measured $\delta^{18}O_{BSi}$ data over the instrumental period and the NPI and PDO index values were binned and averaged within three intervals corresponding to recognized shifts in North Pacific sea-surface temperatures (SSTs) in 1944 CE (to negative PDO conditions) and 1975 CE (to positive PDO conditions) (Khapalova et al., 2018). As the AL and PDO are synoptic-scale patterns primarily impacting climate on multi-decadal timescales (Trenberth and Hurrell, 1994; Mantua et al., 1997), binning $\delta^{18}O_{BSi}$ data to reflect known regime shifts is appropriate for comparing the paleo-data to these modes of variability.

4.1.1 Controls on $\delta^{18}O_{BSi}$

Assuming a fractionation factor of –0.2‰/°C (Brandriss et al., 1998; Moschen et al., 2005; Dodd and Sharp, 2010) between the bottom water of the core site for SIL17-1 (10.6°C) and the youngest sedimentary diatoms at SIL ($\delta^{18}O_{BSi}$ = 28.3‰), $\delta^{18}O_{lake}$ was calculated to within 2.1‰ of the measured value (–7.2‰ calculated versus –9.3‰ measured). The offset between measured and calculated $\delta^{18}O_{lake}$ is unsurprising, in part due to uncertainty in the fractionation factor between water and diatom silica, for which published values range from –0.16‰/°C to –0.49‰/°C (Juillet-Leclerc and Labeyrie, 1987; Brandriss et al., 1998; Moschen et al., 2005; Shemesh et al., 1992; Crespin et al., 2010; Dodd and Sharp, 2010). Furthermore, a growing body of evidence suggests diagenetic alteration may overprint the $\delta^{18}O$ of diatom silica in the decades following sedimentary deposition (Dodd et al., 2017; Tyler et al., 2017; Menicucci et al., 2017). There is no clear solution to account for this possible diagenetic alteration in paleoenvironmental reconstructions, but we acknowledge that it adds uncertainty to any sedimentary $\delta^{18}O_{BSi}$ reconstruction, including at SIL. In one study using marine sedimentary diatoms, a universal correction was applied to each $\delta^{18}O_{BSi}$ value (Menicucci et al., 2019), but this approach does not account for the uncertainty in the duration of diagenetic alteration, which may occur over decades (Dodd et al., 2017) to millions of years (Menicucci et al., 2017). In light of the uncertainties regarding the fractionation between lake water and diatom silica, as well as the potential influence of diagenetic alteration of sedimentary diatom $\delta^{18}O$, the offset between calculated and measured $\delta^{18}O_{lake}$ at SIL is expected, and does not reduce our confidence that the $\delta^{18}O_{BSi}$ dataset is broadly indicative of changes in $\delta^{18}O_{lake}$.

As described above, the temperature-dependent fractionation between diatom silica and lake water is small (~ –0.2‰/°C), meaning it is often damped by larger fluctuations in $\delta^{18}O_{lake}$ that can occur due to changes in both precipitation/evaporation balance (P-E) and $\delta^{18}O_{precip}$ (Leng and Barker, 2006). Therefore, the $\delta^{18}O_{BSi}$ dataset from SIL is interpreted primarily in terms of these hydroclimatic variables, as has been done for other $\delta^{18}O_{BSi}$ records from southern Alaska (Schiff et al., 2009; Bailey et al., 2015; Bailey et al., 2018), rather than in terms of Holocene temperature changes. The $\delta^{18}O_{lake}$ composition of SIL demonstrates it is heavily influenced by evaporative enrichment relative to local meteoric water, where the average $\delta^{18}O_{lake}$ is –8.8‰ (n = 6) and the average $\delta^{18}O$ of ground and river waters, which reflect an average of local meteoric waters, is –15.9‰ (n = 8) (Fig. 5; Table S2).

Combined with aerial photographic evidence for rapid lake-level fluctuations, which also indicates the influence of evaporation (Fig. 1C-D), these data suggest that P-E is likely a key driver of sedimentary $\delta^{18}O_{BSi}$ at SIL. Assuming this condition applies in the past, then sedimentary $\delta^{18}O_{BSi}$ would be sensitive to P-E. The influence of P-E on $\delta^{18}O_{BSi}$ is revealed through shifts during the instrumental period that are negatively correlated with changes in the amount of annual precipitation at Kenai airport (r = –0.81, p = 0.02) (Fig. 10B). This result indicates that during wetter years (higher P-E), less evaporative enrichment results in lower $\delta^{18}O_{lake}$, and subsequent lower $\delta^{18}O_{BSi}$; during drier years (lower P-E), more evaporative enrichment increases $\delta^{18}O_{lake}$ and $\delta^{18}O_{BSi}$.

One major driver of changes in P-E in southern Alaska is the variability in the position and intensity of the AL (Jones et al., 2014; Bailey et al., 2018). Because a stronger AL tends to increase the amount of winter (November – March) precipitation arriving in the Kenai lowlands, wetter winter conditions accompany a strong AL. Increased winter precipitation resulting from a strong AL might result in lower $\delta^{18}O_{lake}$ values at SIL due to higher P-E (indicating an overall wetter climate), but also by increasing the relative annual contribution of isotopically light winter precipitation (compared to summer; Fig. 2).

The AL also modulates the dominant path of storms arriving in the Kenai lowlands, which in turn can alter average $\delta^{18}O_{precip}$. Because a strong AL encourages south-to-north (meridional) transport from the GoA to the Kenai lowlands (Cayan and Peterson, 1989; Mock et al., 1998; Rodionov et al., 2007; Berkelhammer et al., 2012), these storms tend to travel less distance and cross fewer continental barriers before arriving in the Kenai lowlands. Conversely, a weak AL encourages west-to-east (zonal) transport from further west in the North Pacific Ocean. Storms during a weak AL tend to travel greater distances and cross more continental barriers, and therefore are likely to experience more rain-out of ^{18}O, depleting $\delta^{18}O_{precip}$ arriving in the Kenai lowlands. This relation between the AL and $\delta^{18}O_{precip}$ has been corroborated by several isotope-enabled model experiments

(Berkelhammer et al., 2012; Porter et al., 2014). The rain-out effect of ^{18}O due to shifting average storm tracks has an opposing influence on $\delta^{18}O_{lake}$ to that of P-E: a strong AL leads to heavier $\delta^{18}O_{precip}$, and therefore higher $\delta^{18}O_{lake}$, compared to a weak AL (Fig. 3). While there is little instrumental data to support this relation between $\delta^{18}O_{precip}$ and the AL on the Kenai Peninsula, $\delta^{18}O_{precip}$ recorded in Anchorage during the three strongest (2019, 2015, 2016) and weakest (2009, 2011, 2018) AL years from 2005–2018 reveal average $\delta^{18}O_{precip}$ was heavier during years with an anomalously strong AL as indicated by the NPI. During the winter months (November – March), average $\delta^{18}O_{precip}$ was 1.7‰ heavier during the strongest (–18.5‰) versus the weakest (–20.2‰) AL years, and average $\delta^{18}O_{precip}$ was 3.0‰ heavier during the strongest (–15.7‰) versus the weakest (–18.7‰) AL years annually (Bailey et al., 2019).

$\delta^{18}O_{BSi}$ values during the instrumental period reveal the relationship between AL strength and $\delta^{18}O_{precip}$ may apply at SIL: $\delta^{18}O_{BSi}$ is broadly consistent with shifts in the PDO and NPI indices (Fig. 10A), where negative NPI (strong AL) and positive PDO index (associated with strong AL) values correspond to higher $\delta^{18}O_{BSi}$. This relation is further corroborated by the difference in $\delta^{18}O_{precip}$ in Anchorage measured in the strongest and weakest AL years described above (Bailey et al., 2019). This suggests $\delta^{18}O_{BSi}$ reflects changes in storm-track-driven $\delta^{18}O_{precip}$ in addition to P-E, which have opposing influences on the $\delta^{18}O_{lake}$ of SIL and other water bodies in the study area (Fig. 3), making it challenging to constrain the relative importance of these two related hydroclimatic influences in the paleo-data. These opposing influences might also explain the relative stability of $\delta^{18}O_{BSi}$ at SIL, because the decrease in $\delta^{18}O_{BSi}$ resulting from wetter conditions would be balanced by changes in $\delta^{18}O_{precip}$. The offset between $\delta^{18}O_{lake}$ at SIL at local river and ground waters (~7‰; Table S2) is larger than the difference between $\delta^{18}O_{precip}$ in the strongest and weakest AL years (up to 3‰; Bailey et al., 2019). However, the overall range of variability in measured $\delta^{18}O_{precip}$ at Anchorage from 2005–2018 is 31.1‰ (average = –16.5‰; min = –36.8‰; max = –5.7‰; Bailey et al., 2019), indicating that changes in $\delta^{18}O_{precip}$ might be capable of driving larger fluctuations in $\delta^{18}O_{lake}$ if sustained on longer timescales. The relationship between binned $\delta^{18}O_{BSi}$ values with known shifts in the PDO and AL indices demonstrate these modes of variability likely influence lake sediment sequences on multi-decadal timescales, despite the lack of significant correlation on an event-specific basis (Bailey et al., 2019) where storm-to-storm variability and local topography might be more likely to confound the fingerprint of these synoptic-scale patterns.

4.1.2 Controls on BSi

BSi in high altitude/latitude lakes might respond to a number of factors, including length of the ice-free season (McKay et al., 2008), nutrient availability (Perren et al., 2017), dilution by minerogenic material associated with storminess (Krawiec and Kaufman, 2014), or changing water chemistry that can influence preservation (Bradbury et al., 1989). SEM imaging of diatoms in SIL sediments indicates that dissolution is not a factor affecting BSi in this sequence (Fig. 4). At SIL, BSi over the instrumental period is negatively correlated with annual precipitation at Kenai airport (r = –0.66, p = 0.01) (Fig. 10C), with periods of higher precipitation corresponding with lower BSi. This result is consistent with a dilution effect whereby increased storminess in the Kenai lowlands causes increased transport of minerogenic material to the lake, and subsequently dilutes BSi, as has been reported elsewhere in southern Alaska (Krawiec and Kaufman, 2014).

While apparent over the instrumental period, dilution by clastic material related to storminess is unlikely to be the only control on BSi at SIL. For example, BSi and organic matter content inferred from LOI (Anderson et al., 2019) are moderately correlated (r = 0.42, p < 0.01) (Fig. S4). Organic matter (OM) fluctuations typically represent combined autochthonous and allochthonous OM and can therefore be tied to catchment-scale sediment composition and productivity (e.g. Shuman, 2003), changes in lake level (e.g. Digerfeldt et al., 1992), or dilution by minerogenic material (e.g. Nesje and

Dahl, 2001). If OM and BSi differ, then BSi might reflect processes that impact diatoms directly, such as changes in seasonality (Buczkó et al., 2018) or taxon-specific responses of diatoms to changing climate or environmental conditions (Lotter and Hofmann, 2003). The correlation between OM and BSi suggests organic content and diatom abundance in SIL sediments are driven by catchment-scale processes to some extent. However, the highest OM in the lake sediments occurs in the early Holocene (~11.5 – 9.5 ka cal BP) and late Holocene (~2.5 – 0.5 ka cal BP), while the period of highest BSi content occurs from ~6.3 – 4.6 ka cal BP, suggesting some independent controls on OM and BSi have been responsible for fluctuations in these metrics as recorded at SIL on century- to multi-millennial timescales (Fig. 7; Fig. S4), and these controls may not have been stable over the course of the sediment sequence. For example, relatively high OM from ~11.5 – 9.5 ka cal BP might reflect heightened organic input from the *Populus-Alnus-Salix* hardwood forest that occupied the region surrounding SIL prior to the arrival of *Picea* (Anderson et al., 2019). Increasing BSi from ~9 – 6 ka cal BP might be related to increasing summer temperature, reflected by the chironomid-based reconstruction from nearby Rainbow Lake (Clegg et al., 2011).

4.2 Holocene hydroclimate and environmental change

4.2.1 Pleistocene-Holocene transition (~12.3 – 11 ka cal BP)

Age-model uncertainties in the basal sediments of the SIL cores make it difficult to extrapolate results older than ~12.3 ka cal BP (Fig. 6). The continuous deposition of organic sediments after ~12.3 ka cal BP is roughly coincident with the inferred lake-level rise during the middle of the Younger Dryas (12.2 ka cal BP) at Discovery Pond, 22 km to the north (Kaufman et al., 2010). Lake level likely started rising prior to this at SIL, as the top of the basal inorganic unit is ~20 cm lower than the sediments dated to ~12.3 ka cal BP, but age model uncertainties preclude an exact assessment of when this occurred.

The oldest diatomaceous sediments at SIL (~11.9 ka cal BP) contain a high relative abundance of *S. pinnata* (PC1; Fig. 8; Fig. 11A), a small, pioneering, fragiliarioid species typical of lakes in recently stabilized landscapes (Smol et al., 2005; Hausmann and Pienitz, 2009). The dominance of *P. saprophila*, a large benthic diatom, might also indicate that lake levels were low enough to yield a proportionately extensive littoral zone, allowing a generally rare benthic diatom to succeed in this environment (Wolin and Duthie, 1999). BSi content remains low (< 5%) throughout this interval (Fig. 11C), most likely due to cold temperatures and turbid waters in the recently deglaciated landscape prohibiting large diatom blooms.

The $\delta^{18}O_{BSi}$ values show large excursions during the Pleistocene-Holocene transition (Fig. 11D): $\delta^{18}O_{BSi}$ decreases from +29.2‰ at ~12 ka cal BP to +26.2‰ (the lowest recorded $\delta^{18}O_{BSi}$) at ~11.5 ka cal BP, then increases to +30.7‰ at ~11 ka cal BP. These changes in $\delta^{18}O_{BSi}$ occur during a major vegetation transition to hardwood forest inferred from the SIL pollen record (Anderson et al., 2019). Large climate shifts inferred from proxy data during the late YD and earliest Holocene have been observed in other records from this region, including at nearby Horse Trail Fen, where inferred $\delta^{18}O$ of environmental water was substantially lower from 11.7 – 10.8 ka cal BP than during the following ~2 ka cal BP (Jones et al., 2019) (Fig. 11E). At Hundred Mile Lake in the Matanuska Valley, Yu et al. (2008) also found positive excursions in $\delta^{18}O_{carbonate}$ from *Pisidium* shells, ostracods, and *Chara* encrustations in the earliest Holocene (~11.7 – 11.4 ka cal BP), followed by deviations in $\delta^{18}O_{carbonate}$, organic matter, carbonate, and silicate content from ~11.2 – 10.9 ka cal BP during a period of inferred earliest Holocene warmth. At Lone Spruce Pond in southwestern Alaska, shifts in BSi as well as $\delta^{13}C$ and $\delta^{15}N$ of organic matter occur between ~12 – 11.5 ka cal BP (Kaufman et al., 2012), and are associated with a warming climate. The mechanism for these excursions in the late YD and earliest Holocene is unclear, though Kaufman et al. (2010) suggest that a strengthened AL in the latter half of the YD promoted wetter and warmer climate conditions across southern Alaska, a possibility that is echoed by Jones et al. (2019). While the precise cause of the changes in $\delta^{18}O_{BSi}$ at SIL is not certain, it seems that a rapidly changing hydroclimate and environment are important features of the glacial-interglacial transition, and that atmospheric circulation patterns may be one of the drivers.

4.2.2 Early and middle Holocene (~11 – 4.5 ka cal BP)

Dated transitions from minerogenic sediments to terrestrial peat in satellite fens surrounding SIL from ~9.5 – 7.7 ka cal BP (Fig. 11F) indicate that the water level at SIL declined during the early Holocene to several meters lower compared to the late Holocene water level, as revealed by the ice-shoved rampart analyses. The ~2 m fen profiles of wet sedge-dominated peat indicate a generally rising water level throughout the mid and into the late Holocene, where the rising zone of peat accumulation tracked the rising lake level. One lake sediment core that captures the upper ~6 ka cal BP from SIL (SIL17-1) shows a basal beach sand (Fig. S1), indicating lake level was rising following an early Holocene low stand.

In the earliest Holocene, the SIL diatom assemblage is dominated by facultatively planktonic and large benthic taxa. By ~10.4 ka cal BP, the relative abundance of these habitat types diminishes, giving way to a high relative abundance of *D. stelligera* (PC2; Fig. 8; Fig. 11A), a small planktonic diatom that has been observed to be related to increases in lake nutrient content at other sites (Law et al., 2015). The increase in *D. stelligera* at SIL coincides with the highest relative abundances of *Alnus* pollen (Anderson et al., 2019), a genus known to increase local nitrogen availability (Shaftel et al., 2011). Perren et al. (2017) documented the same relationship between *D. stelligera* and *Alnus* at Lone Spruce Pond in southwestern Alaska, where they peak later in the Holocene. Given the evidence for lowered lake levels at SIL (described above) and warm, dry conditions elsewhere in the Kenai lowlands (Anderson et al., 2006; Jones et al., 2009; Anderson et al., 2019) at this time, the increase in *D. stelligera* is likely related to the aforementioned landscape and soil processes rather than to a high lake level *per se*, as the higher relative abundance of planktonic diatoms might suggest (Wolin and Duthie, 1999). Following these high abundances of *D. stelligera*, the diatom assemblage is dominated by facultatively planktonic taxa, making interpretations of lake-level changes difficult, but indicating continued nitrogen enrichment (McGowan et al., 2005; Scheffer and van Nes, 2007). At ~6 ka cal BP there is an increase in the percentage of *D. stelligera* and *Aulacoseira* spp., potentially due to rising lake levels increasing the water column depth and providing more habitat for colonization by these planktonic diatom taxa.

Low and progressively increasing BSi from ~11.5 – 8 ka cal BP likely reflects the prevalent and increasing presence of *Alnus* on the landscape (Anderson et al., 2019) (Fig. 11B), which fixes nitrogen and encourages diatom blooms (Perren et al., 2017) (Fig. 11C). The highest BSi in the dataset then occur between ~6.3 and ~4.6 ka cal BP, approximately concurrent with the highest pollen concentrations (Anderson et al., 2019), though these high BSi values are interrupted by a minimum at ~5.5 ka cal BP. These fluctuations might represent the influence of changes in runoff, which controls mineral delivery to the lake, coupled with increased land cover and productivity as a result of a shift to a wetter climate. Changes in runoff might also impact the delivery of other limiting nutrients for diatom growth, such as silicon and phosphorus, which would cause changes in diatom abundance. The arrival and establishment of *Picea mariana* at ~4.5 ka cal BP (Anderson et al., 2019) is thought to be associated with a shift to wetter climate (Hu et al., 1996; Lynch et al., 2002), providing an additional line of evidence for a shift in hydroclimate at this time.

Persistent fluctuations in $\delta^{18}O_{BSi}$ during most of the early and mid Holocene (Fig. 11D) are difficult to attribute to any one hydroclimate variable. Jones et al. (2014, 2019) interpreted elevated $\delta^{18}O$ of both total organic matter (TOM) and cellulose of peat and rapid peat accumulation in nearby Horse Trail Fen to represent a weakened AL, an increased contribution of summer precipitation, and overall wet conditions in the early Holocene. The inverse relation between the Horse Trail Fen and SIL $\delta^{18}O$ values (Fig. 11D-E) might be explained by the different seasonal influences on $\delta^{18}O_{TOM}$ in peat and $\delta^{18}O_{BSi}$ in lake sediment. Peat accumulation is heavily dependent on summer moisture, and therefore likely reflects a disproportionate influence of summer precipitation compared to climate proxies found in lake sediments, which instead are more likely to reflect annual average or winter-dominated conditions as represented by $\delta^{18}O_{lake}$ (Jones et al., 2014). LaBrecque and Kaufman (2016) also found evidence for the advance of an outlet glacier from ~10.8 – 9.8 ka cal BP at Emerald Lake in the Kenai Mountains, which they interpret as indicative of either lower summer temperature or higher winter snowfall. In contrast, several studies (Anderson et al., 2006; Jones et al., 2009; Anderson et al., 2019) have interpreted the early Holocene as a dry period in the Kenai lowlands based on pollen and plant macrofossil evidence. The early-mid Holocene SIL $\delta^{18}O_{BSi}$ record does little to corroborate or reject any of these hypotheses regarding hydroclimate, though the diatom assemblage and fen peat data support the notion that lake levels were low and progressively rose following the early Holocene.

$\delta^{18}O_{BSi}$ values remained relatively low (mean = +29.1‰, n = 41) until ~5.7 ka cal BP, when they increased steadily until reaching sustained higher values (~ +31.2‰) by ~4.5 ka cal BP, encompassing the largest step-wise shift in the Holocene (Fig. 11D). This observed shift to higher $\delta^{18}O_{BSi}$ at ~4.5 ka cal BP could be interpreted to reflect a decrease in P-E, or drier conditions. However, periodic late Holocene increases in the relative abundance of planktonic diatoms at SIL, the presence of peats in satellite fens following the early Holocene low stand, and regional evidence for wetter conditions at this time (Anderson et al., 2006) are all lines of evidence that challenge this interpretation. If increased evaporation (decreased P-E) is not responsible for increasing $\delta^{18}O_{lake}$ and $\delta^{18}O_{BSi}$ at ~4.5 ka cal BP, another possible driver of the shift would be an increase in $\delta^{18}O_{precip}$ values. Isotopically heavier precipitation could have occurred due to a change in average storm track trajectories associated with a shift to a stronger AL (Fig. 3), which would favor meridional atmospheric flow and therefore relatively less rain-out of ^{18}O (as described in Section 4.1.1). Numerous recent studies (Barron and Anderson, 2011; Jones et al., 2014; Bailey et al., 2018) have suggested that the AL strengthened and increased in variability between 5 – 4 ka cal BP, including at nearby Horse Trail Fen (Jones et al., 2014; 2019) (Fig. 11E), which is the only other full Holocene $\delta^{18}O$ record from the Kenai lowlands. While we cannot unilaterally attribute the increase in $\delta^{18}O_{BSi}$ from ~5.5 – 4.5 ka cal BP at SIL to an increase in $\delta^{18}O_{precip}$ rather than to decreased P-E based on the datasets presented in this study, several lines of evidence indicate the climate became wetter and the AL strengthened at ~4.5 ka cal BP, suggesting that a stronger AL is the more likely driver of this shift. The aforementioned datasets that have previously identified a shift in AL activity at this time span from southwestern Yukon to Adak Island (Fig. 1A), and together with SIL $\delta^{18}O_{BSi}$ indicate a synoptic-scale shift in North Pacific ocean-atmosphere circulation and terrestrial climate conditions around the boundary between the mid and late Holocene.

4.2.3 Following the increase in $\delta^{18}O_{BSi}$ at ~4.5 ka cal BP (~4.5 – 1 ka cal BP)

Diatom assemblages following the ~4.5 ka cal BP transition remain diverse, though the relative abundance of planktonic taxa increases slightly from ~4 to 1 ka cal BP, suggesting a shift to a deeper water column (Wolin and Duthie, 1999) (Fig. 11A). Intermittent increases in *Aulacoseira* spp., which form heavy colonies requiring turbulence for suspension in the water column to remain in the photic zone (Rühland et al., 2008; Lotter et al., 2010), could indicate the presence of persistent stronger winds associated with storminess throughout the late Holocene (Wang et al., 2008; Andrén et al., 2015; Solovieva et al., 2015).

Following the highest Holocene $\delta^{18}O_{BSi}$ values between ~4.7 – 2.7 ka cal BP (mean = +31.2‰, n = 12), $\delta^{18}O_{BSi}$ decreased from ~2.7 – 1 ka cal BP (mean = +30.2‰, n = 13), but still remained elevated relative to the early and mid-Holocene (mean = +29.2‰, n = 54). The sustained enriched $\delta^{18}O$ values likely indicate the continued contribution of ^{18}O enriched precipitation due to the shift to dominantly stronger AL conditions (Fig. 11D). The slight decreasing trend in $\delta^{18}O$ values could be interpreted as representative of a progressively weakening AL over the late Holocene (Fig. 3). However, BSi decreases over this interval, potentially indicating an increase in storminess and subsequent BSi dilution by mineral matter transported to the lake during storms (Fig. 11C). Elevated percentages of planktonic taxa in the late Holocene might also indicate higher lake levels associated with increased precipitation. Charcoal accumulation rates from nearby Paradox Lake (Anderson et al., 2006) also reveal fire frequency declined in the late Holocene, implying regional climate was wetter at this time. The neoglacial advance of glaciers in the Kenai Mountains in the last ~4 ka cal BP also indicates regionally wetter conditions that promoted the accumulation of snow and ice (Barclay et al., 2009; Kaufman et al., 2016). Additionally, ice-shoved ramparts above the modern and inferred paleo-shorelines of SIL indicate lake levels were higher than either the early Holocene or the present by ~1.5 ka cal BP (Fig. 11F). Therefore, it is possible that following the initial change in precipitation source water at ~4.5 ka cal BP, the influence of P-E on $\delta^{18}O_{lake}$ became more prominent. Though the opposing effects of changes in $\delta^{18}O_{precip}$ and P-E cannot be definitively teased apart, the evidence for wetter conditions at SIL, in the Kenai lowlands, and across eastern Beringia (Kaufman et al., 2016) supports the interpretation of an increase in precipitation during the late Holocene. We therefore interpret the overall decrease in $\delta^{18}O_{BSi}$ over the late Holocene, combined with decreasing BSi and periodic, intermittent increases in the abundance of planktonic diatoms, to indicate an overall wetter climate during this interval, though these changes in climate conditions cannot be unequivocally attributed to AL strength.

4.2.4 Last millennium (~1 ka cal BP – present)

$\delta^{18}O_{BSi}$ values decreased during the last millennium (mean = +28.3‰, n = 27), reaching the lowest value since 11.5 ka cal BP (+26.5‰ at 1996 CE) (Fig. 11D). The initial decrease starting at ~1 ka cal BP might have been related to the documented advance of glaciers in the First Millennium CE in south-central Alaska (Barclay et al., 2009) and throughout the northeastern Pacific Cordilleran (Reyes et al., 2006), suggesting colder and wetter conditions throughout this region during the last millennium, consistent with lower $\delta^{18}O_{BSi}$ associated with both a P-E isotope imprint, and possibly cooler air temperatures that could lower $\delta^{18}O_{precip}$ (Dansgaard, 1964). Superimposed on the decreasing trend are excursions to lower $\delta^{18}O_{BSi}$ at ~1250 – 1400 CE and ~1700 – 1750 CE (Fig. 12). These shifts correspond to documented glacial advances (Fig. 12; Wiles and Calkin, 1993; Wiles et al., 1999; Daigle and Kaufman, 2009; LaBrecque and Kaufman, 2016) throughout the western Prince William Sound region that have been attributed to early and late stages of the Little Ice Age (LIA), and are therefore likely associated with changing regional hydroclimate conditions, which impacted both glaciers and lakes. Given the negative correlation between $\delta^{18}O_{BSi}$ and annual precipitation at Kenai airport over the instrumental record (Fig. 10B), it follows that these negative $\delta^{18}O_{BSi}$ excursions might represent wet intervals during the LIA that resulted in glacier expansion. Additionally, ice-shoved rampart evidence for higher-than-modern lake levels persists from ~1090 CE until ~1550 CE (Fig. 11F). In light of the agreement between SIL $\delta^{18}O_{BSi}$ and evidence for regional glacial advances, we interpret the continued and enhanced overall decreasing trend in $\delta^{18}O_{BSi}$, coupled with decreasing BSi, as increasingly wet conditions in the last millennium.

Since 2000 CE, both $\delta^{18}O_{BSi}$ values and BSi increased, likely as a result of lowered lake levels, reduced P-E (for $\delta^{18}O_{BSi}$), as well as increased temperatures and longer ice-free seasons (for BSi). The percentage of planktonic diatoms also decreased, while facultatively planktonic taxa such as *S. pinnata* (PC1; Fig. 8) increased to their highest abundances in the Holocene, particularly in surface sediments. An increased abundance of *S. pinnata* has been previously associated with nutrient enrichment (McGowan et al., 2005; Scheffer and van Nes, 2007) and disturbance (Anderson, 2000), which is consistent with warming, drying, fire, and road construction on this landscape in recent decades. The elevations of dated terrestrial peats from perched satellite fens also indicate that current conditions are the driest in the Holocene, with modern lake levels well below both dated late Holocene ice-shoved ramparts and inferred early Holocene lake level minima (Fig. 11F). These dramatic recent changes have occurred at a time of unprecedented rates of climate warming (Alaska Climate Research Center, 2009), suggesting the landscape and lakes in the Kenai lowlands will likely be subjected to continued alteration.

5 Conclusions

The multi-proxy record of environmental change from Sunken Island Lake in the Kenai lowlands reflects regional hydroclimate conditions over the Holocene. In the Kenai lowlands, a stronger AL is associated with an increase in storms that track from the south and deliver more precipitation that is relatively enriched in ^{18}O. An increase in $\delta^{18}O_{BSi}$ at ~4.5 ka cal BP implies an increase in $\delta^{18}O_{precip}$ associated with AL strength, supporting prior work showing enhanced AL strength around 4 ka cal BP (Barron and Anderson, 2011; Jones et al., 2014; Bailey et al., 2018). Multiple lines of evidence support the interpretation of an increasingly wet late Holocene (beginning at ~4.5 ka cal BP) compared to the early and mid Holocene, including high shorelines and ice-shoved ramparts, decreased BSi, and increased planktonic diatom abundances between 4 and 1 ka cal BP. This trend towards wetter conditions during the late Holocene has been reversed in the 21st Century, when multiple lines of evidence indicate rapidly falling lake levels and decreased P-E. Despite the uncertainty and challenges associated with reconciling multiple, competing influences on this oxygen isotope record, our study demonstrates how the use of multiple hydroclimate indicators (BSi, diatom flora, and $\delta^{18}O_{BSi}$) can help evaluate the relative contributions of these influences, rather than attributing changes in $\delta^{18}O_{BSi}$ to only one primary influence (i.e. AL variability). Specifically, intervals of lower BSi and/or higher planktonic diatom relative abundances clarify interpretations of the mid to late Holocene $\delta^{18}O_{BSi}$ data where it might otherwise have been more difficult to discern changes in $\delta^{18}O_{precip}$ from changes in P-E. Given the complexity of relating shifts in synoptic-scale patterns to $\delta^{18}O_{precip}$ (Bailey et al., 2019), this approach of contemplating a more complex explanation of $\delta^{18}O$ paleo-data may lead to fewer conflicting $\delta^{18}O$ interpretations among paleoclimate studies.

6 Conflict of Interest

The authors declare that the research was conducted in the absence of any commercial or financial relationships that could be construed as a potential conflict of interest.

7 Author Contributions

EB led the study with guidance from DSK, co-led fieldwork, purified diatom oxygen isotope samples, prepared and analyzed diatom assemblage samples, analyzed water isotope samples, prepared samples for geochronological analyses, and wrote the original manuscript. DSK co-led field work and reviewed early versions of the manuscript. ACGH provided expert assistance with the interpretations of the diatom isotope and flora analyses. EEB participated in fieldwork and conducted analyses on the SIL fen cores and ice-shoved rampart samples. RSA participated in fieldwork, provided previously acquired sediments and data, and identified plant macrofossils for dating. MJL oversaw the analysis of the diatom oxygen isotope samples at the British Geological Survey. SAS produced and interpreted the BSi data. SEM analysed and interpreted $^{210}Pb/^{137}Cs$ gamma data. All co-authors read and edited the manuscript.

8 Funding

This project was funded by National Science Foundation award 1602106 to DSK, and by grants and scholarships to EB from the Geological Society of America (GSA), GSA Limnogeology Division, the Phycological Society of America, LacCore/CSDCO, and the School of Earth and Sustainability at Northern Arizona University.

9 Acknowledgments

We wish to thank the Kenai Natives Association for permitting our sediment and water sampling at Sunken Island Lake; the U.S. Fish and Wildlife Service, Kenai National Wildlife Refuge for their interest in this research and for assisting with field work; Eric Sandberg and Molly McCormick for housing our field teams and assisting with water and sediment sampling; Nicholas McKay for assistance with GeoChronR and for valuable insights that improved this manuscript; David Fortin and Ann Jade Wong for assistance with field work; Dick Reger for describing the ice-shoved rampart soil profiles; Katherine Whitacre, Kathryn Geyer, and Mackenzie Sanchez for assistance with laboratory work; Chris Ebert for assisting with the preparation of the ^{14}C samples; UC Irvine Keck Carbon Cycle Laboratory for analyzing the ^{14}C samples; Jack Lacey and Hilary Sloane for analysis of the diatom oxygen isotopes at the British Geological Survey; Jamie Brown of the Colorado Plateau Isotope Lab for analyzing the water samples; LacCore/CSDCO for assisting with Initial Core Description; and Polar Field Services/CH2MHill for outfitting our field teams. We are grateful for suggestions from Jonathan Tyler and one anonymous reviewer that greatly improved this manuscript.

10 References

Alaska Climate Research Center (2009). Temperature changes in Alaska. http://climate.gi.alaska.edu/ClimTrends/Change/TempChange.html [accessed 11 Dec 2019]

Anderson, N.J. (2000). Diatoms, temperature and climatic change. *Eur. J. Phycol.* 35, 307-314. doi:10.1080/09670260010001735911

Anderson, L., Abbott, M.B., Finney, B.P., and Burns, S.J. (2005). Regional atmospheric circulation change in the North Pacific during the Holocene inferred from lacustrine carbonate oxygen isotopes, Yukon Territory, Canada. *Quat. Res.* 64, 21-35. doi:10.1016/j.yqres.2005.03.005

Anderson, R.S., Hallett, D.J., Berg, E., Jass, R.B., Toney, J.L., de Fontaine, C.S., and DeVolder, A. (2006). Holocene development of Boreal forests and fire regimes on the Kenai Lowlands of Alaska. *Holocene* 16(6), 791-803. doi:10.1191/0959683606hol966rp

Anderson, R.S., Berg, E., Williams, C., and Clark, T. (2019). Postglacial vegetation community change over an elevational gradient on the western Kenai Peninsula, Alaska: pollen records from Sunken Island and Choquette Lakes. *J. Quat. Sci.* 34, 309-322. doi:10.1002/jqs.3102

Andrén, E., Klimaschewski, A., Self, A.E., Amour, N.S., Andreev, A.A., Bennett, K.D., Conley, D.J., Edwards, T.W.D., Solovieva, N., and Hammarlund, D. (2015). Holocene climate and environmental change in north-eastern Kamchatka (Russian Far East), inferred from a multi-proxy study of lake sediments. *Global Planet. Change* 134, 41-54. doi:10.1016/j.gloplacha.2015.02.013

Appleby, P. (2001). "Chronostratigraphic techniques in recent sediments," in Tracking Environmental Change Using Lake Sediments, Vol. 1. eds. W. Last and J. Smol. (Dordrecht, The Netherlands: Kluwer Academic Publishers), 171-203

Bailey, H.L., Kaufman, D.S., Henderson, A.C.G., and Leng, M.J. (2015). Synoptic scale controls on the $\delta^{18}O$ in precipitation across Beringia. *Geophys. Res. Lett.* 42, 4608-4616. doi:10.1002/2015GL063983

Bailey, H.L., Kaufman, D.S., Sloane, H.J., Hubbard, A.L., Henderson, A.C.G., Leng, M.J., Meyer, H., and Welker, J.M. (2018). Holocene atmospheric circulation in the central North Pacific: A new terrestrial diatom and $\delta^{18}O_{diatom}$ dataset from the Aleutian Islands. *Quat. Sci. Rev.* 194, 27-38. doi:10.1016/j.quascirev.2018.06.027

Bailey, H.L., Klein, E.S., and Welker, J.M. (2019). Synoptic and mesoscale mechanisms driver winter precipitation $\delta^{18}O$/ $\delta^{2}H$ in south-central Alaska. *J. Geophys. Res.-Atmos.* 124, 4252-4266. doi:10.1029/2018JD030050

Barclay, D.J., Wiles, G.C., and Calkin, P.E. (2009). Tree-ring crossdates for a First Millennium AD advance of Tebenkof Glacier, southern Alaska. *Quat. Res.* 71, 22-26. doi:10.1016/j.yqres.2008.09.005

Barron, J. A., and Anderson, L. (2011). Enhanced Late Holocene ENSO/PDO expression along the margins of the eastern North Pacific. *Quat. Int.* 235, 3-12. doi:10.1016/j.quaint.2010.02.026

Berkelhammer, M.B., Stott, L.D., Yoshimura, K., Johnson, K., and Sinha, A. (2012). Synoptic and mesoscale controls on the isotopic composition of precipitation in the western United States. *Clim. Dynam.* 38, 433-454. doi:10.1007/s00382-011-1262-3

Blaauw, M., and Christen, J.A. (2011). Flexible paleoclimate age-depth models using an autoregressive gamma process. *Bayesian Anal.* 6(3), 457-474. doi:10.1214/11-BA618

Boes, E., Van Daele, M., Moeraut, J., Schmidt, S., Jensen, B.J.L, Praet, N., Kaufman, D., Haessler, P., Loso, M.G., and De Batist, M. (2018). Varve formation during the past three centuries in three large proglacial lakes in south-central Alaska. *Geol. Soc. Am. Bull.* 130, 757-774. doi:10.1130/B31792.1

Bradbury, J.P., Forester, R.M., and Thompson, R.S. (1989). Late Quaternary paleolimnology of Walker Lake, Nevada. *J. Paleolimnol.* 1(4), 249-267. doi:10.1007/BF00184000

Brandriss, M.E., O'Neil, J.R., Edlund, M.B., and Stoermer, E.F. (1998). Oxygen isotope fractionation between diatomaceous silica and water. *Geochim. Cosmochim. Acta* 62, 1119–1125. doi:10.1016/S0016-7037(98)00054-4

Bretherton, C.S., Widmann, M., Dymnikov, V.P., Wallace, J.M., and Bladé, I. (1998). The effective number of spatial degrees of freedom of a time-varying field. *J. Climate* 12, 1990-2009. doi:10.1175/1520-0442(1999)012<1990:TENOSD>2.0.CO;2

Brewer, T.S., Leng, M.J., Mackay, A.W., Lamb, A.L., Tyler, J.T., Marsh, N.G., 2008. Unraveling contamination signals in biogenic silica oxygen isotope composition: the role of major and trace element geochemistry. *J. Quat. Sci.* 23(4), 321-330. doi:10.1002/jqs.1171

Buczkó, K., Szurdoki, E., Braun, M., and Magyari, E. (2018). Reconciling diverse diatom-based lake responses to climate change in four mountain lakes in the South-Carpathian Mountains during the last 17 kyrs. *Quat. Int.* 477, 117-137. doi:10.1016/j.quaint.2017.03.013

Cayan, D.R., and Peterson, D.H. (1989). "The influence of North Pacific circulation on streamflow in the West," in Aspects of Climate Variability in the Pacific and Western Americas, Vol. 55, ed. D.H. Peterson (Washington, DC: American Geophysical Union), 375–398

Clegg, B.F., Kelly, R., Clarke, G.H., Walker, I.R., and Hu, F.S. (2011). Nonlinear response of summer temperature to Holocene insolation forcing in Alaska. *P. Natl. Acad. Sci. USA.* 108(48), 19299-19304. doi:10.1073/pnas.1110913108

Crespin, J., Sylvestre, F., Alexandre, A., Sonzogni, C., Pailles, C., and Perga, M-E. (2010). Re-examination of the temperature-dependent relationship between $\delta^{18}O_{diatoms}$ and $\delta^{18}O_{lake\ water}$ and implications for paleoclimate inferences. *J. Paleolimnol.* 44, 547-557. doi:10.1007/s10933-010-9436-2

Daigle, T.A., and Kaufman, D.S. (2009). Holocene climate inferred from glacier extent, lake sediment and tree rings at Goat Lake, Kenai Mountains, Alaska, USA. *J. Quat. Sci.* 24, 33-45. doi:10.1002/jqs.1166

Dansgaard, W. (1964). Stable isotopes in precipitation. *Tellus*, 16(4), 436–468. doi:10.1111/j.2153-3490.1964.tb00181.x

Dean, W.E. (1974). Determination of carbonate and organic matter in calcareous sediments and sedimentary rocks by loss on ignition; comparison with other methods. *J. Sed. Res*. 44(1), 242-248. doi:10.1306/74D729D2-2B21-11D7-8648000102C1865D

Digerfeldt, G., Almendinger, J.E., and Björck, S. (1992). Reconstruction of past lake levels and their relation to groundwater hydrology in the Parkers Prairie sandplain, west-central Minnesota. *Palaeogeogr. Paleocl.* 94, 99-118. doi:10.1016/0031-0182(92)90115-L

Dodd, J.P., and Sharp, Z.D. (2010). A laser fluorination method for oxygen isotope analysis of biogenic silica and a new oxygen isotope calibration of modern diatoms in freshwater environments. *Geochim. Cosmochim. Acta* 74(4), 1381-1390. doi:10.1016/j.gca.2009.11.023

Dodd, J.P., Sharp, Z.D., Fawcett, P.J., Brearley, A.J., McCubbin, F.M., 2012. Rapid post-mortem maturation of diatom silica oxygen isotope values. *Geochem. Geophys.* 13(9), Q09014. doi:10.1029/2011GC004019

Fisher, D., Osterberg, E., Dyke, A., Dahl-Jensen, D., Demuth, M., Zdanowicz, C., Bourgeois, J., Koerner, R.M., Mayewski, P., Wake, C., Kreutz, K., Steig, E., Zheng, J., Yalcin, K., Goto-Azuma, K., Luckman, B., and Rupper, S. (2008). The Mt Logan Holocene - late Wisconsinan isotope record: tropical Pacific - Yukon connections. *Holocene* 18, 667-677. doi:10.1177/0959683608092236

Foged N. (1971). Diatoms found in a bottom sediment sample from a small deep lake on the Northern Slope, Alaska. *Nova Hedwigia* 21(1-4): 923-1034

Foged, N. (1981). Diatoms in Alaska. *Bibliotheca Phycologica* 53, 1-317

Grimm, E.C. (1987). Coniss - a Fortran-77 program for stratigraphically constrained cluster-analysis by the method of incremental sum of squares. *Computat. Geosci.* 13, 13-35. doi:10.1016/0098-3004(87)90022-7

Grimm, E.C. (2015). TILIA Software. Version 2.1.1. https://www.tiliait.com/download/

Hamilton, S., and Shennan, I. (2005). Late Holocene great earthquakes and relative sea-level change at Kenai, southern Alaska. *J. Quat. Sci.* 20, 95-111. doi:10.1002/jqs.903

Hausmann, S., and Pienitz, R. (2009). Seasonal water chemistry and diatom changes in six boreal lakes of the Laurentian Mountains (Québec, Canada): impacts of climate and timber harvesting. *Hydrobiologia* 635(1), 1-14. doi:10.1007/s10750-009-9855-0

Hu, F.S., Brubaker, L.B., and Anderson, P.M. (1996). Boreal ecosystem development in the northwestern Alaska Range since 11,000 yr B.P. *Quat. Res.* 45(2), 188-201. doi:10.1006/qres.1996.0019

Jones M.C., Peteet D.M., Kurdyla D., and Guilderson, T. (2009). Climate and vegetation history from a 14,000-year peatland record, Kenai Peninsula, Alaska. *Quat. Res.* 72, 207–217. doi:10.1016/j.yqres.2009.04.002

Jones, M.C., Wooller, M., and Peteet, D.M. (2014). A deglacial and Holocene record of climate variability in south-central Alaska from stable oxygen isotopes and plant macrofossils in peat. *Quat. Sci. Rev.* 87, 1-11. doi:10.1016/j.quascirev.2013.12.025

Jones, M.C., Anderson, L., Keller, K., Nash, B., Littell, V., Wooller, M., and Jolley, C.A. (2019). An assessment of plant species differences on cellulose oxygen isotopes from two Kenai Peninsula Alaska peatlands: implications for hydroclimatic reconstructions. *Front. Earth Sci.* 7(25), 1-25. doi:10.3389/feart.2019.00025

Juillet-Leclerc, A., Labeyrie, L. (1987). Temperature dependence of the oxygen isotopic fractionation between diatom silica and water. *Earth Planet. Sci. Lett.* 84, 69–74. doi:10.1016/0012-

821X(87)90177-4

Kaufman D.S., Anderson R.S., Hu F.S., Berg, E., and Werner, A. (2010). Evidence for a variable and wet Younger Dryas in southern Alaska. *Quat. Sci. Rev.* 29: 1445–1452. doi:10.1016/j.quascirev.2010.02.025

Kaufman, D.S., Axford, Y., Anderson, R.S., Lamoureux, S.F., Schindler, D.E., Walker, I.R., and Werner, A. (2012). A multi-proxy record of the Last Glacial Maximum and last 14,500 years of paleoenvironmental change at Lone Spruce Pond, southwestern Alaska. *J. Paleolimnol.* 48, 9-26. doi:10.1007/s10933-012-9607-4

Kaufman, D.S., Axford, Y.L., Henderson, A.C.G., McKay, N.P., Oswald, W.W., Saenger, C., Anderson, R.S., Bailey, H.L., Clegg, B., Gajewski, K., Hu, F.S., Jones, M.C., Massa, C., Routson, C.C., Werner, A., Wooller, M.J., and Yu, Z. (2016). Holocene climate changes in eastern Beringia (NW North America) — A systematic review of multi-proxy evidence. *Quat. Sci. Rev.* 147, 312-339. doi:10.1016/j.quascirev.2015.10.021

Khapalova, E.A., Jandhyala, V.K., Fotopoulos, S.B., and Overland, J.E. (2018). Assessing change-points in surface air temperature over Alaska. *Front. Enviro. Sci.* 6(121), 1-17. doi:10.3389/fenvs.2018.00121

Koning, E., Gehlen, M., Flank, A.M., Calas, G., Epping, E., 2007. Rapid post-mortem incorporation of aluminum in diatom frustules: evidence from chemical and structural analyses. *Marine Chem.* 106, 208-222. doi:10.1016/j.marchem.2006.06.009

Krammer, K., and Lange-Bertalot, H. (1986-1991). Bacillariophyceae Band 1-4. Stuttgart: Gustav Fischer Verlag.

Krawiec, A.C.L., and Kaufman, D.S. (2014). Holocene storminess inferred from sediments of two lakes on Adak Island, Alaska. *Quat. Res.* 82, 73-84. doi:10.1016/j.yqres.2014.02.007

LaBrecque, T.S., and Kaufman, D.S. (2016). Holocene glacier fluctuations inferred from lacustrine sediment, Emerald Lake, Kenai Peninsula, Alaska. *Quat. Res.* 85, 34-43. doi:10.1016/j.yqres.2015.11.004

Law, A.C., Anderson, N.J., and McGowan, S. (2015). Spatial and temporal variability of lake ontogeny in south-western Greenland. *Quat. Sci. Rev.* 126, 1-16. doi:10.1016/j.quascirev.2015.08.005

Leng, M.J., and Barker, P.A. (2006). A review of the oxygen isotope composition of lacustrine diatom silica for palaeoclimate reconstruction. *Earth-Sci. Rev.* 75, 5-27. doi:10.1016/j.earscirev.2005.10.001

Leng, M.J., and Sloane, H.J. (2008). Combined oxygen and silicon isotope analysis of biogenic silica. *J. Quat. Sci.* 23, 313-319. doi:10.1002/jqs.1177

Lotter, A.F., and Hofmann, G. (2003). “The development of the late-glacial and Holocene diatom flora in Lake Sedmo Rilsko (Rila Mountains, Bulgaria),” in Aspects of Palynology and Palaeoecology, ed. S. Tonkov (Moscow, Russia: Pensoft Publishers), 171-183

Lotter, A.F., Pienitz, R., and Schmidt, R. (2010). “Diatoms as indicators of environmental change in subarctic and alpine regions,” in The Diatoms: Application for the Environmental and Earth Sciences, eds. J.P. Smol and E.F. Stoermer (Cambridge: United Kingdom: Cambridge University Press), 97-115

Lynch, J.A., Clark, J.S., Bigelow, N.H., Edwards, M.E., and Finney, B.P. (2002). Geographic and temporal variations in fire history in boreal ecosystems of Alaska. *J. Geophys. Res.-Atmos.*108, NO. D1, 8152. doi:10.1029/2001JD000332

Mann, D.G., McDonald, S.M., Mayer, M.M., Droop, S.J.M., Chepurnov, V.A., Loke, R.E., Ciobanu, A., and Du Buf, J.M.H. (2004). The *Sellaphora pupula* species complex (Bacillariophyceae): Morphometric analysis, ultrastructure and mating data provide evidence for five new species. *Phycologia* 43, 459-482. doi:10.2216/i0031-8884-43-4-459.1

Mantua, N.J., Hare, S.R., Zhang, Y., Wallace, J.M., and Francis, R.C. (1997). A Pacific interdecadal climate oscillation with impacts on salmon production. *B. Am. Meteorol. Soc.* 78, 1069-1079. doi:10.1175/1520-0477(1997)078<1069:APICOW>2.0.CO;2

Menicucci, A.J., Spero, H.J., Matthews, J., and Parikh, S.J. (2017). Influence of exchangeable oxygen on biogenic silica oxygen isotope data. *Chem. Geol*. 466, 710-721. doi:10.1016/j.chemgeo.2017.07.020

Menicucci, A.J., Thunell, R.C., and Spero, H.J. (2019). 220 year diatom δ^{18}O reconstruction of the Guaymas Basin thermocline using microfluorination. *Palaeogeogr. Paleocl.* 35(2), e2019PA003749. doi:10.1029/2019PA003749

McGowan, S., Patoine, A., Graham, M.D., and Leavitt, P. (2005). Intrinsic and extrinsic controls on lake phytoplankton synchrony as illustrated by algal pigments. *SIL Proceedings 1922-2010*, 29(2), 794-798. doi:10.1080/03680770.2005.11902787

McKay, N.P., Kaufman, D.S., and Michelutti, N. (2008). Biogenic silica concentration as a high resolution, quantitative temperature proxy at Hallet Lake, south-central Alaska. *Geophys. Res. Lett.* 35, L05709, doi:10.1029/2007GL032876

McKay, N.P., Emile-Geay, J., Heiser, C., and Khinder, D. (2018). GeoChronR development repository. Retrieved from http://dx.doi.org/10.5281/zenodo.60812. doi:10.5281/zenodo.60812

McLaughlin, R.B., and Stone, J.L. (1986). Some late Pleistocene diatoms of the Kenai Peninsula, Alaska. *Nova Hedwigia* 82, 1-148

Mock, C.J., Bartlein, P.J., and Anderson, P.M. (1998). Atmospheric circulation patterns and spatial climatic variations in Beringia. *Int. J. Climatol.* 10, 1085-1104. doi:10.1002/(SICI)1097-0088(199808)18:10<1085::AID-JOC305>3.0.CO;2-K

Mortlock, R.A., and Froelich, P.N. (1989). A simple method for the rapid determination of biogenic opal in pelagic marine sediments. *Deep-Sea Res.* 36, 1415-1426. doi:10.1016/0198-0149(89)90092-7

Morley, D.W., Leng, M.J., Mackay, A.W., Sloane, H J., Rioual, P., and Battarbee, R.W. (2004). Cleaning of lake sediment samples for diatom oxygen isotope analysis. *J. Palaeolimnol*. 31, 391–401. doi:10.1023/B: JOPL.0000021854.70714.6b

Moschen, R., Lücke, A., and Schleser, G.H. (2005). Sensitivity of biogenic silica oxygen isotopes to changes in surface water temperature and paleoclimatology. *Geophys. Res. Lett.* 32, L07708. doi:10.1029/2004GL22167

Nesje, A., and Dahl, S.O. (2001). The Greenland 8200 cal. yr BP event detected in loss-on-ignition profiles in Norwegian lacustrine sediment sequences. *J. Quat. Sci.* 16(2), 155-166. doi:10.1002/jqs.567

Overland, J.E., Adams, J.M., and Bond, N.A. (1999). Decadal variability of the Aleutian Low and its relation to high-latitude circulation. *J. Clim.* 12, 1542-1548. doi:10.1175/1520-0442(1999)012<1542:DVOTAL>2.0.CO;2

Paillard, D., Labeyrie, L., and Yiou, P. (1996). Macintosh program performs time-series analysis. *Eos* 77(39), 379. doi:10.1029/96EO00259

Perren, B.B., Axford, Y., and Kaufman, D.S. (2017). Alder, nitrogen, and lake ecology: terrestrial-aquatic linkages in the postglacial history of Lone Spruce Pond, southwestern Alaska. *PloS ONE* 12(1), e0169106. doi:10.1371/journal.pone.0169106

Praet, N., Moernaut, J., Van Daele, M., Boes, E., Haeussler, P., Strupler, M., Schmidt, S., Loso, M., and Batist, M. (2017). Paleoseismic potential of sublacustrine landslide records in a high-seismicity setting (south-central Alaska). *Mar. Geol.* 384, 103-119. doi:10.1016/j.margeo.2016.05.004

Porter, T.J., Pisaric, M.F.J., Field, R.D., Kokelj, T.W.D., deMontigny, P., Healy, R., and LeGrande, A.N. (2014). Spring-summer temperatures since AD 1780 reconstructed from stable oxygen isotope ratios in white spruce tree-rings from the Mackenzie Delta, northwestern Canada. *Clim. Dynam.* 42, 771-785. doi:10.1007/s00382-013-1674-3

Reimer, P.J., Bard, E., Bayliss, A., Beck, J.W., Blackwell, P.G., Ramsey, C.B., Buck, C.E., Cheng, H., Edwards, R.L., Friedrich, M., Grootes, P.M., Guilderson, T.P., Haflidason, H., Hajdas, I., Hatté, C., Heaton, T.J., Hoffmann, D.L., Hogg, A.G., Hughen, K.A., Kaiser, K.F., Kromer, B., Manning, S.W., Niu, M., Reimer, R.W., Richards, D.A., Scott, E.M., Southon, J.R., Staff, R.A., Turney, C.S.M., van der Plicht, J. (2013). IntCal13 and Marine13 radiocarbon age calibration curves, 0-50,000 years cal BP. *Radiocarbon* 55(4), 1869-1887. doi:10.2458/azu_js_rc.55.16947

Reger, R.D., Sturmann, A.G., Berg, E.E., and Burns, P.A.C. (2007). A guide to the late Quaternary history of northern and western Kenai Peninsula, Alaska: Guidebook 8. Anchorage, Alaska: State of Alaska Department of Natural Resources, Division of Geological and Geophysical Surveys.

Reyes, A.V., Wiles, G.C., Smith, D.J., Barclay, D.J., Allen, S., Jackson, S., Larocque, S., Laxton, S., Lewis, D., Calkin, P.E., and Clague, J.J. (2006). Expansion of alpine glaciers in Pacific North America in the first millennium A.D. *Geology* 34(1), 57-60. doi:10.1130/G21902.1

Rodionov, S.N., Overland, J.E., and Bond, N.A. (2005). Spatial and temporal variability of the Aleutian climate. *Fish. Oceanogr.* 14, 3-21. doi:10.1111/j.1365-2419.2005.00363.x

Rodionov, S.N., Bond, N.A., and Overland, J.E. (2007). The Aleutian Low, storm tracks, and winter climate variability. *Deep-Sea Res. II* 54, 2560-2577. doi:10.1016/j.dsr2.2007.08.002

Rühland, K., Paterson, A.M., and Smol, J.P. (2008). Hemispheric-scale patterns of climate-related shifts in planktonic diatoms from North American and European lakes. *Glob. Change Biol.* 14(11), 2740e2754. doi:10.1111/j.1365-2486.2008.01670.x

Scheffer, M., and van Nes, E.H. (2007). Shallow lakes theory revisited: various alternative regimes driven by climate, nutrients, depth and lake size. *Hydrobiologia* 584, 455-466. doi:10.1007/s10750-007-0616-7

Schiff, C., Kaufman, D.S., Wolfe, A.P., Dodd, J., and Sharp, Z. (2009). Late Holocene storm-trajectory changes inferred from the oxygen isotope composition of lake diatoms, south Alaska. *J. Paleolimnol.* 41, 189-208. doi:10.1007/s10933-008-9261-z

Shaftel, R.S., King, R.S., and Back, J.A. (2011). Alder cover drives nitrogen availability in Kenai lowland headwater streams, Alaska. *Biogeochemistry* 107, 135-148. doi:10.1007/s10533-010-9541-3

Shemesh, A., Charles, C.D., and Fairbanks, R.G. (1992). Oxygen isotopes in biogenic silica: global changes in ocean temperature and isotopic composition. *Science* 256, 1434–1436. doi:10.1126/science.256.5062.1434

Shuman, B. (2003). Controls on loss-on-ignition variation in cores from two shallow lakes in the northeastern United States. *J. Paleolimnol.* 30, 371-385. doi:10.1023/B:JOPL.0000007226.68831e3

Smol, J.P., Wolfe, A.P., Birks, H.J.B., Douglas, M.S., Jones, V.J., Korhola, A., Pienitz, R., Rühland, K., Sorvari, S., Antoniades, D., and Brooks, S.J. (2005). Climate-driven regime shifts in the biological communities of arctic lakes. *P. Natl. Acad. Sci. USA.* 102(12), 4397e4402. doi:10.1073/pnas.0500245102

Solovieva, N., Klimaschewski, A., Self, A.E., Jones, V.J., Andren, E., Andreev, A.A., Hammarlund, D., Lepskaya, E.V., and Nazarova, L. (2015). The Holocene environmental history of a small coastal lake on the north-eastern Kamchatka Peninsula. *Global Planet. Change* 134, 55e66. doi:10.1016/j.gloplacha.2015.06.010

Spaulding, S.A., Bishop, I.W., Edlund, M.B., Lee, S. and Potapova, M. (2019). Diatoms of North America. https://diatoms.org/ [accessed 11 Dec 2019]

ter Braak, C.J.F., and Prentice, I.C. (1988). A theory of gradient analysis. *Adv. Ecol. Res.* 18, 271e317. doi:10.1016/S0065-2504(03)34003-6

Trenberth, K.E., and Hurrell, J.W. (1994). Decadal atmosphere-ocean variations in the Pacific. *Clim. Dynam.* 9, 303-319. doi:10.1007/BF00204745

Tyler, J.J., Sloane, H.J., Rickaby, R.E.M., Cox, E.J., and Leng, M.J. (2017). Post-mortem oxygen isotope exchange within cultured diatom silica. *Rapid. Commun. Mass Sp.* 31(20), 1749-1760. doi:10.1002/rcm.7954

Wang, L., Lu, H., Liu, J., Gu, Z., Mingram, J., Chu, G., Li, J., Rioual, P., Negendank, J.F., Han, J., and Liu, T. (2008). Diatom-based inference of variations in the strength of Asian winter monsoon winds between 17,500 and 6000 calendar years BP. *J. Geophys. Res.-Atmos.* 113, D2101. doi:10.1029/2008JD010145

Wiles, G.C., and Calkin P.E. (1993). Neoglacial fluctuations and sedimentation of an iceberg-calving glacier resolved with tree rings (Kenai Fjords National Park, Alaska). *Quat. Int*. 18, 35-42. doi:10.1016/1040-6182(93)90051-G

Wiles, G.C., Barclay, D.J., and Calkin, P.E. (1999). Tree-ring-dated 'Little Ice Age' histories of maritime glaciers from western Prince William Sound, Alaska. *Holocene* 9(2), 163-173. doi:10.1191/095968399671927145

Wolin, J.A., and Duthie, H.C. (1999). "Diatoms as indicators of water level change in freshwater lakes," in The Diatoms: Application for the Environmental and Earth Sciences, eds. J.P. Smol and E.F. Stoermer (Cambridge: United Kingdom: Cambridge University Press), 183–202

Yu, Z.C., Walker, K.N., Evenson, E.B., and Hadjas, I. (2008). Late glacial and early Holocene climate oscillations in the Matanuska Valley, south-central Alaska. *Quat. Sci. Rev.* 27, 148-161. doi:10.1016/j.quascirev.2007.02.020

11 Supplementary Material

See attached Supplementary Figures and Tables as well as Supplementary Data (Excel sheet).

12 Data Availability Statement

The depths and ages for all sediment cores used in this study can be found in the attached data supplement. The BSi and $\delta^{18}O_{BSi}$ data can be found in the attached data supplement, and at the World Centre for Paleoclimatology. The diatom assemblage data can be found at the Neotoma Paleoecology Database. *Note to editor: Data will be transferred when the manuscript is accepted for publication.*

Figures and Tables

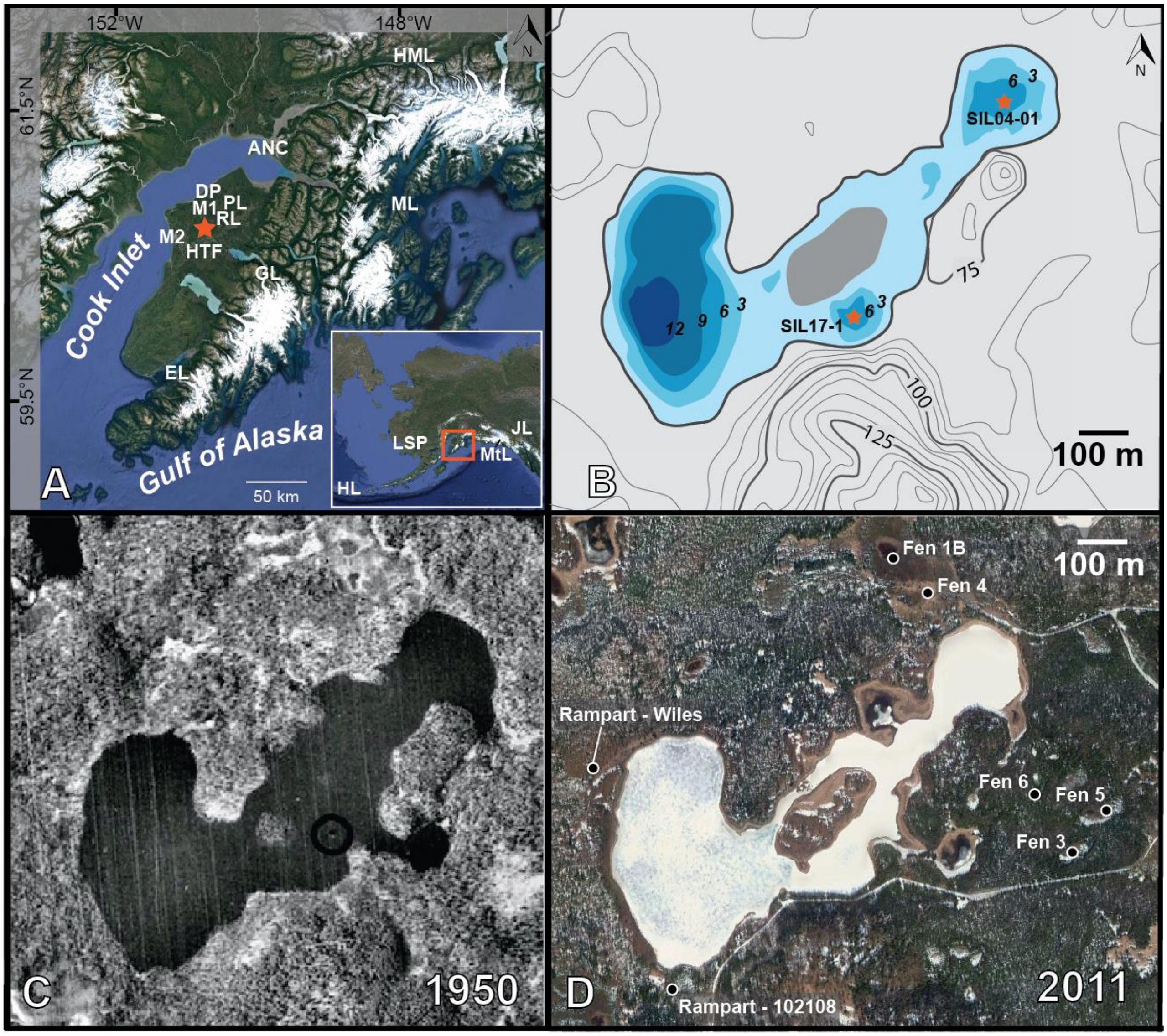

Figure 1: (A) Location of Sunken Island Lake in the Kenai lowlands indicated by the orange star. Locations of the following sites are marked: Anchorage (ANC), Kenai Moose Pens SNOTEL meteorological station (M1), Kenai airport meteorological station (M2), Heart Lake (HL; Bailey et al., 2018), Lone Spruce Pond (LSP; Kaufman et al., 2012), Mount Logan (MtL; Fisher et al., 2008), Jellybean Lake (JL; Anderson et al., 2005), Emerald Lake (EL; LaBrecque and Kaufman, 2016), Horse Trail Fen (HTF; Jones et al., 2014, 2019), Discovery Pond (DP; Kaufman et al., 2010), Paradox Lake (PL; Anderson et al., 2006), Rainbow Lake (RL; Clegg et al., 2011), Goat Lake (GL;

Daigle and Kaufman, 2009), Mica Lake (ML; Schiff et al., 2009); and Hundred Mile Lake (HML; Yu et al., 2008). Images from Google Earth. (B) Bathymetric map of Sunken Island Lake, with water depths shown in increments of 3 m, and contour lines in increments of 5 m. Orange stars indicate sites of sediment cores analyzed for this study. (C-D) Aerial photographs of Sunken Island Lake in 1950 CE (DeVolder, *pers. comm.*) (C) and in 2011 CE (Google Earth) (D). Locations of sampled satellite fens and ice-shoved ramparts are shown in (D).

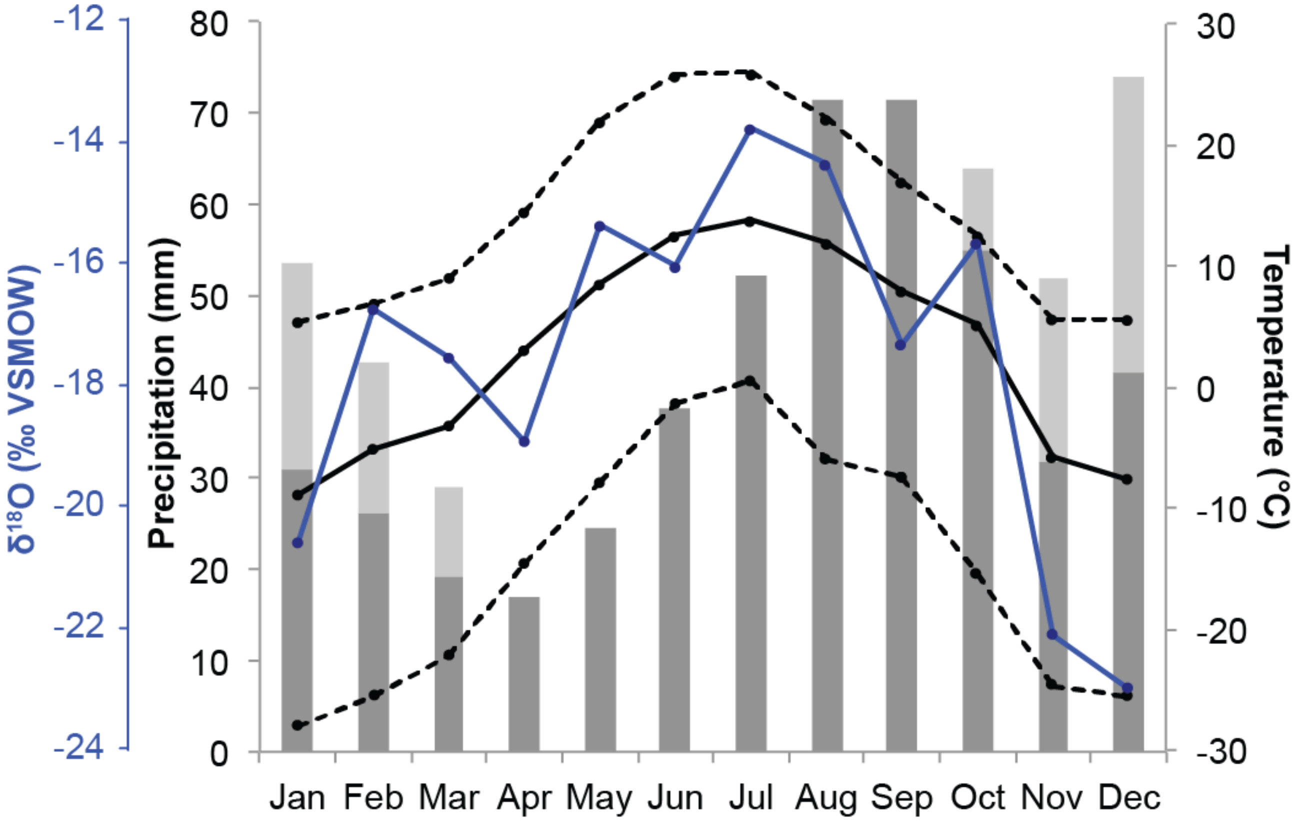

Figure 2: (A) Meteorological data from the Kenai Moose Pens SNOTEL site in Soldotna, AK (https://www.wcc.nrcs.usda.gov/index.html), showing the average (solid line), high (upper dashed line), and low (lower dashed line) temperatures alongside average monthly precipitation (dark gray bars) and average monthly snow-water equivalent (SWE; light gray bars) for 1995 – 2019 CE. (B) The same precipitation and SWE data as in (A) shown alongside monthly $\delta^{18}O_{precipitation}$ from the Tideview Station in Anchorage for 2005 – 2017 CE (Bailey et al., 2019).

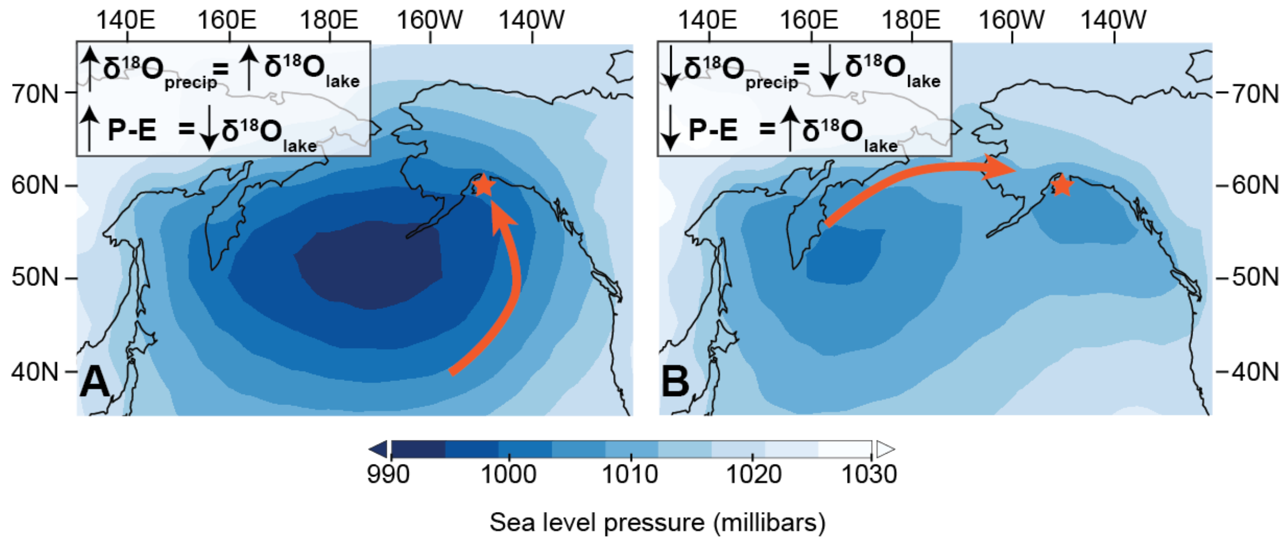

Figure 3: Study region showing the relation between Aleutian Low strength and associated effect on precipitation/evaporation balance P-E, $\delta^{18}O_{precipitation}$ and $\delta^{18}O_{lake}$. Average sea level pressure for the ten strongest (A) and weakest (B) Aleutian Low years from 1951 – 2000 CE is shown, as indicated by the North Pacific Index (after Rodionov et al., 2007). Orange arrows represent the tendency of storm tracks in the ten strongest and weakest Aleutian Low years for the same ten strongest (A) and weakest (B) AL years (Rodionov et al., 2007). The competing influences of $\delta^{18}O_{precip}$ and P-E on $\delta^{18}O_{lake}$ at Sunken Island Lake are described in white text.

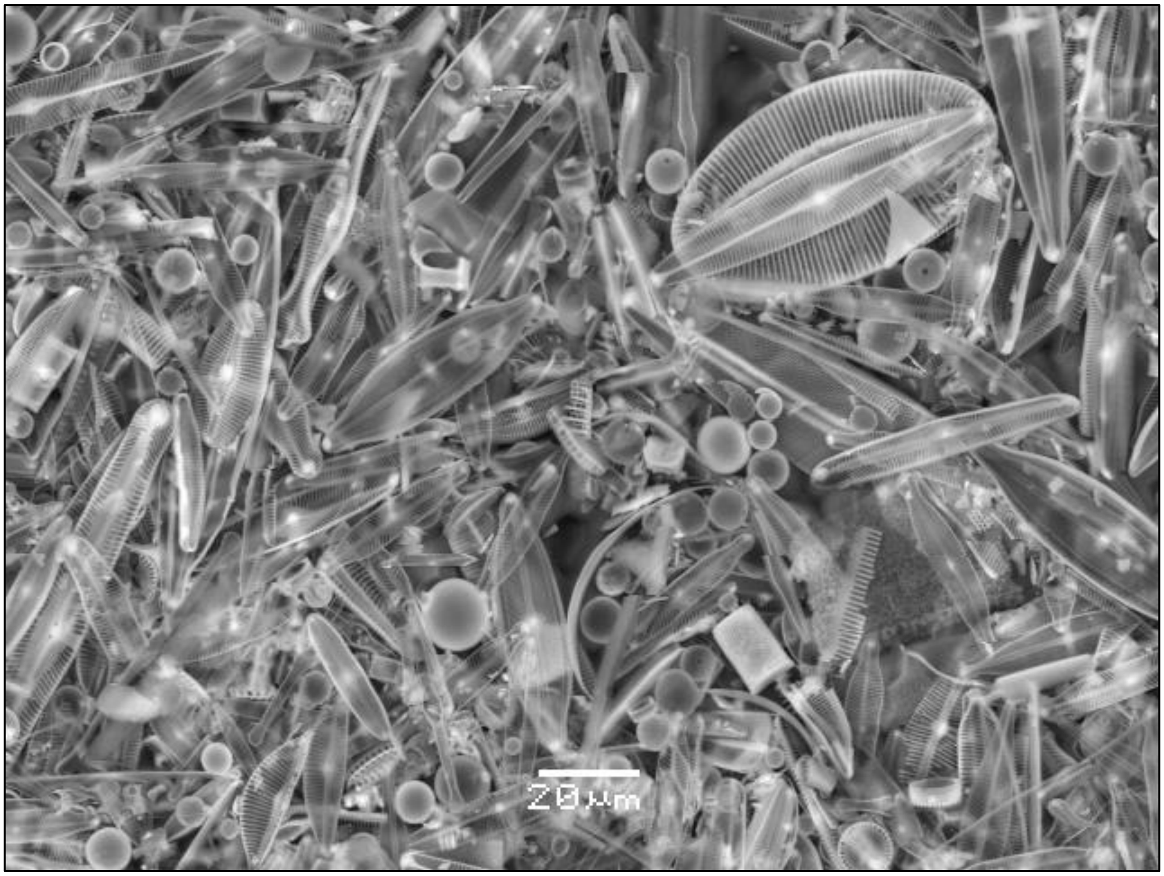

Figure 4: Scanning electron microprobe image of purified biogenic silica from 383.5 cm below lake floor (5662 ± 86 a cal BP) at Sunken Island Lake. Spherical features are chrysophyte cysts.

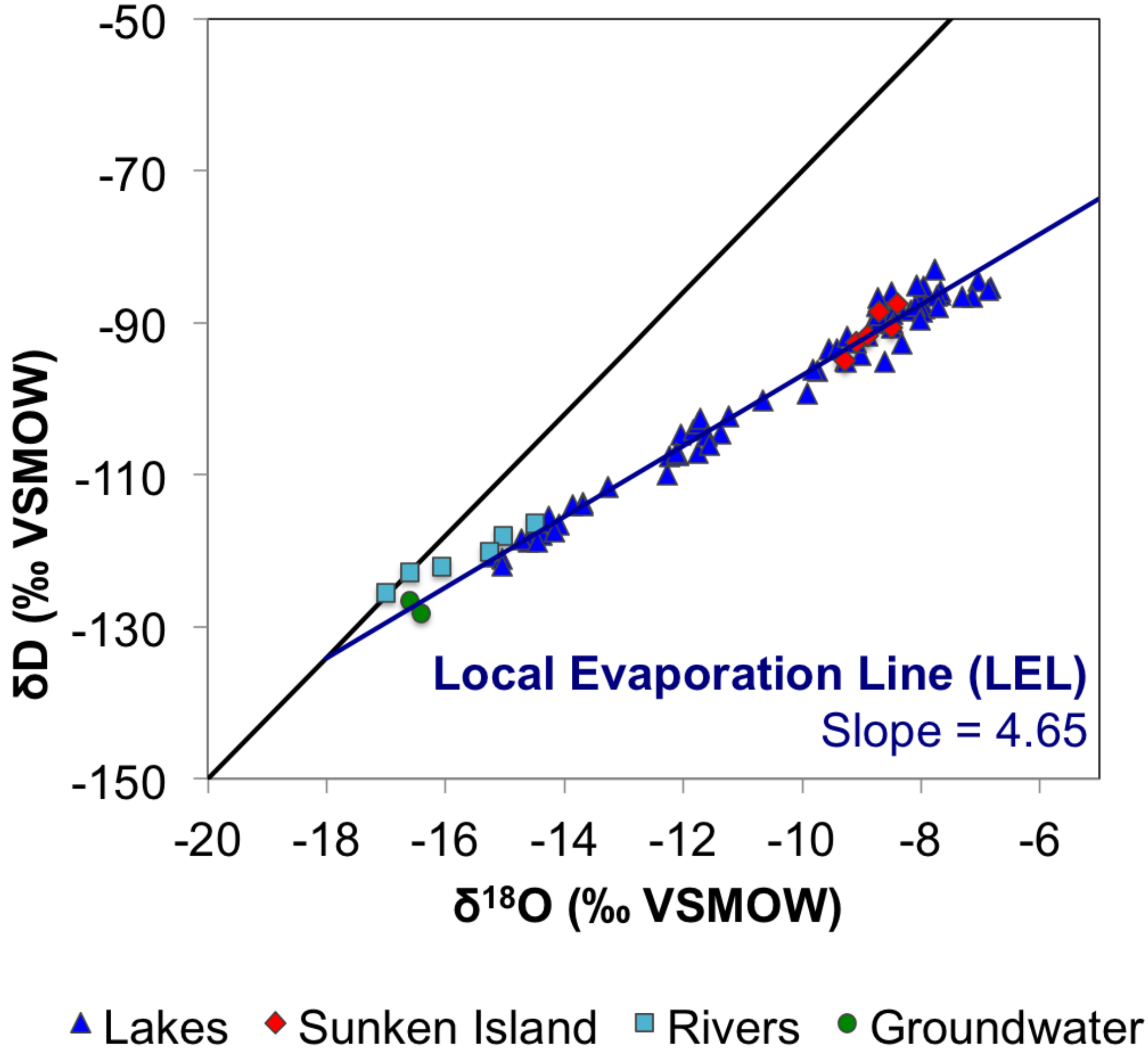

Figure 5: Water isotope data for lakes, rivers, and groundwater in the Kenai lowlands collected between 2017 and 2018 CE, with Local Evaporation Line (LEL; dark blue) plotted for all lake water samples, and the Global Meteoric Water Line (GMWL; black). Data are in Table S2.

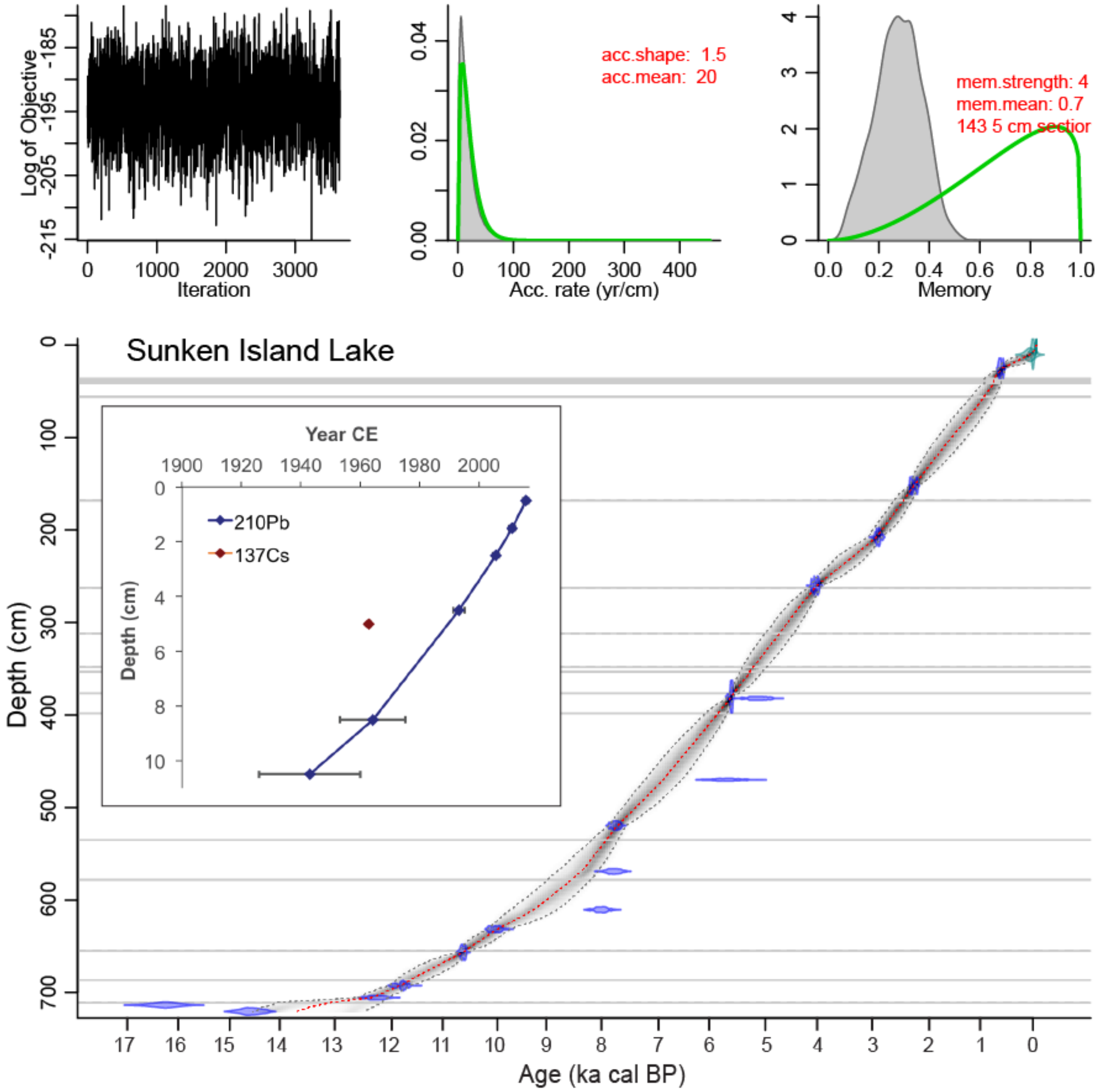

Figure 6: Age-depth model for Sunken Island Lake master core (SIL-MC), created using Bacon (v2.2; Blaauw and Christen, 2011). Gray horizontal lines mark visible tephra deposits that were assumed to have been deposited instantaneously. The depths and basal ages of these layers are in Table S3. Inset shows ^{210}Pb and ^{137}Cs profiles of the near surface (data in Fig. S3 and Table S1).

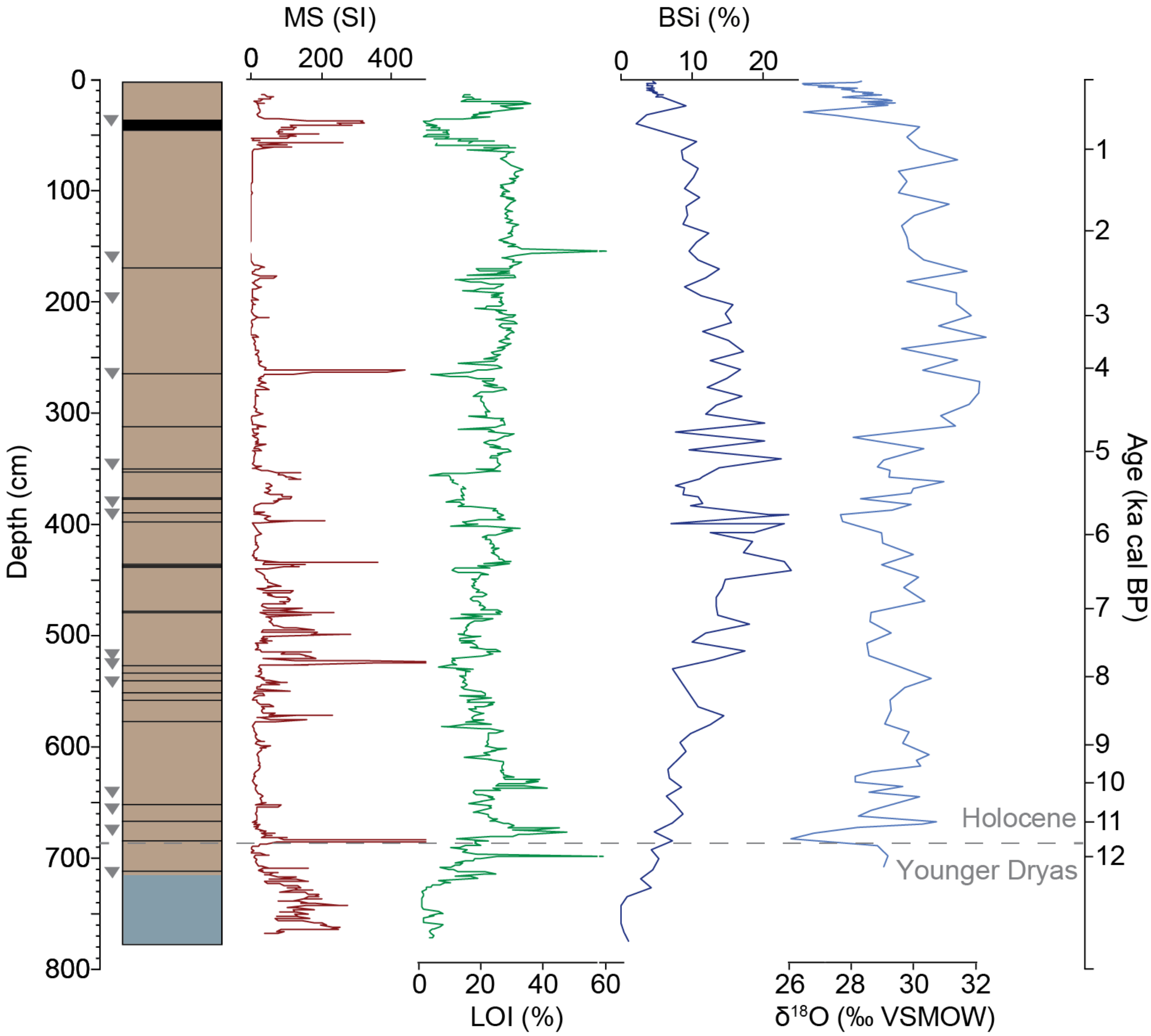

Figure 7: Stratigraphy of Sunken Island Lake master core (SIL-MC) with magnetic susceptibility (MS), loss on ignition (LOI), and biogenic silica (BSi). The ambient lake sediment (brown) is dominantly gyttja; macroscopically visible tephras are shown as black bands, and basal gray clay and sand is indicated in blue. Age scale is based on the age model shown in Fig. 6. Gray triangles show calibrated ^{14}C ages prior to 13 ka cal BP shown in Table 1. Dashed gray line shows boundary between the Younger Dryas and the Holocene (11.7 ka cal BP).

1023 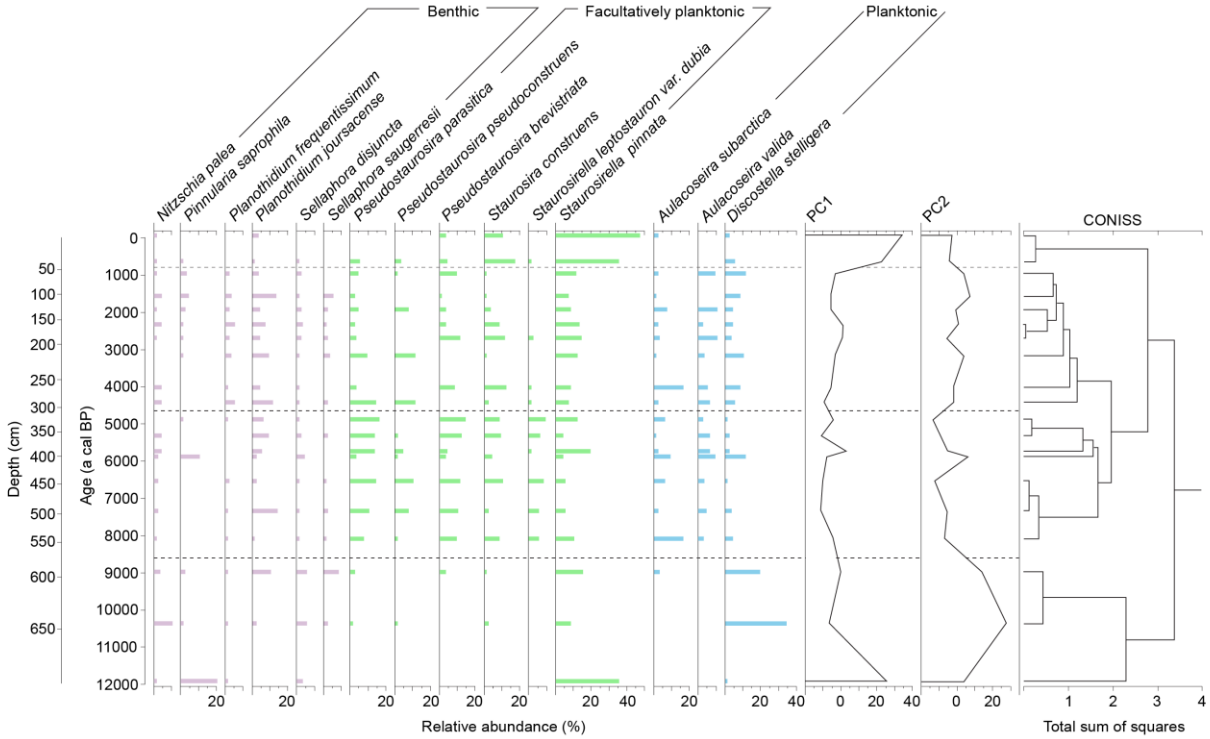

1024 **Figure 8**: Relative abundance of 15 dominant diatom taxa in Sunken Island Lake core SIL-MC.

1025 CONISS-designated zones are indicated by dashed lines. Analyzed and plotted using Tilia (v.2.1.1)

1026 (Grimm, 2015).

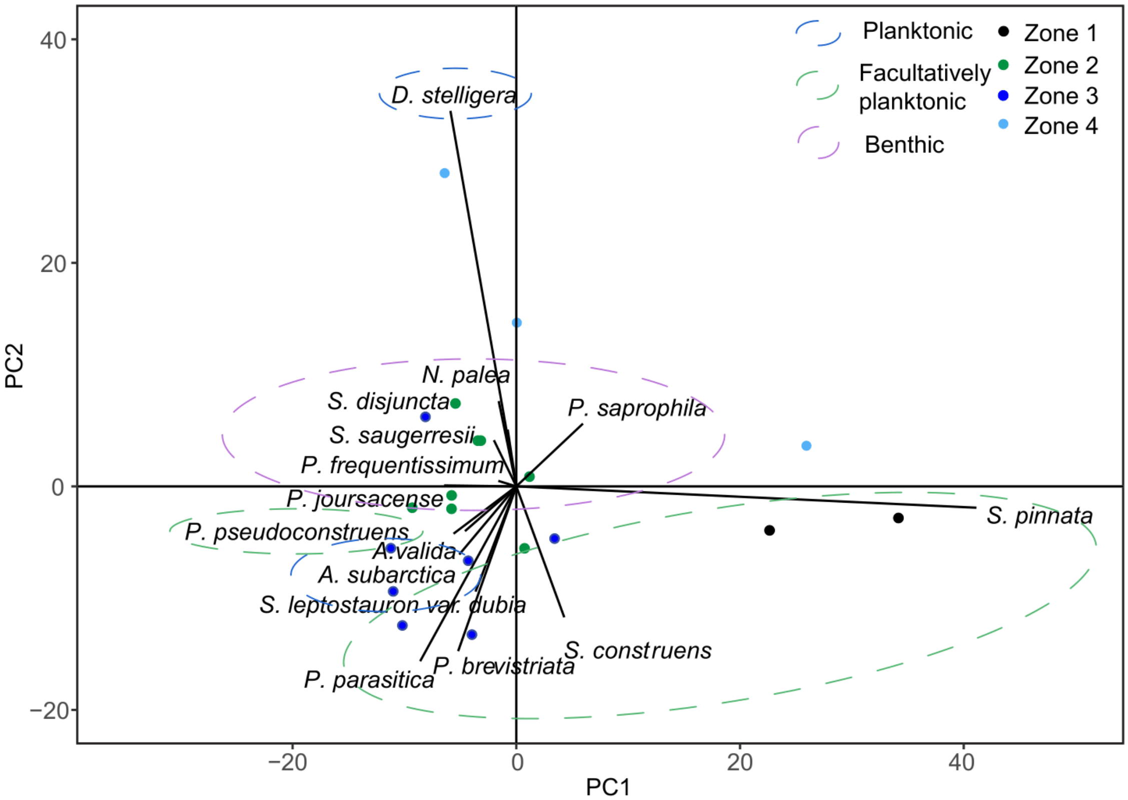

Figure 9: Principal component analysis (PCA) of diatom assemblages by sample. CONISS zone is indicated by dot color, and habitat types (after Spaulding et al., 2019) are enclosed in dashed circles. PC1 explains 41.9% of the variance in the dataset, and PC2 explains 23.5%.

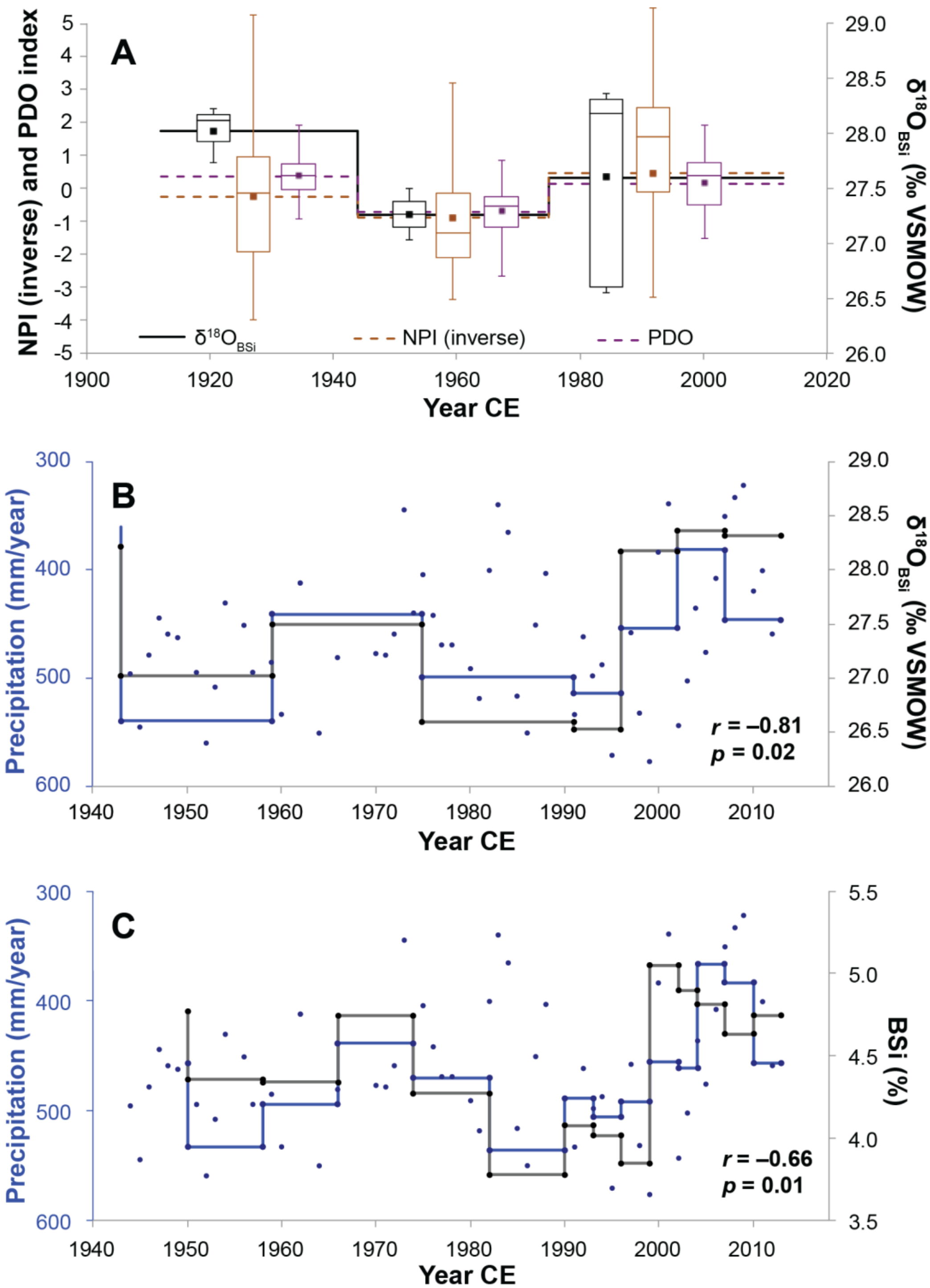

Figure 10: Comparison between instrumental climate data and proxy data from Sunken Island Lake for the period of 1900-2015 CE. (A) $\delta^{18}O_{BSi}$ compared with the North Pacific Index (NPI) and the Pacific Decadal Oscillation (PDO) index (data from https://climatedataguide.ucar.edu and http://research.jisao.washington.edu/pdo/ respectively). The three intervals represent known PDO

regime shifts (Khapalova et al., 2018); index values are averaged over each interval. (B) $\delta^{18}O_{BSi}$ and (C) BSi compared with total annual precipitation (mm/year) at Kenai airport (data from http://climate.gi.alaska.edu/acis_data). Data were binned in panels B and C using the Analyseries software package (Paillard et al., 1996). Binned data are shown by thick lines, while dots are individual data points. The highest and lowest precipitation data points are not shown in the range of data displayed in this figure. Note change in x-axis scale following panel A, and inverse y-axes in panels B and C.

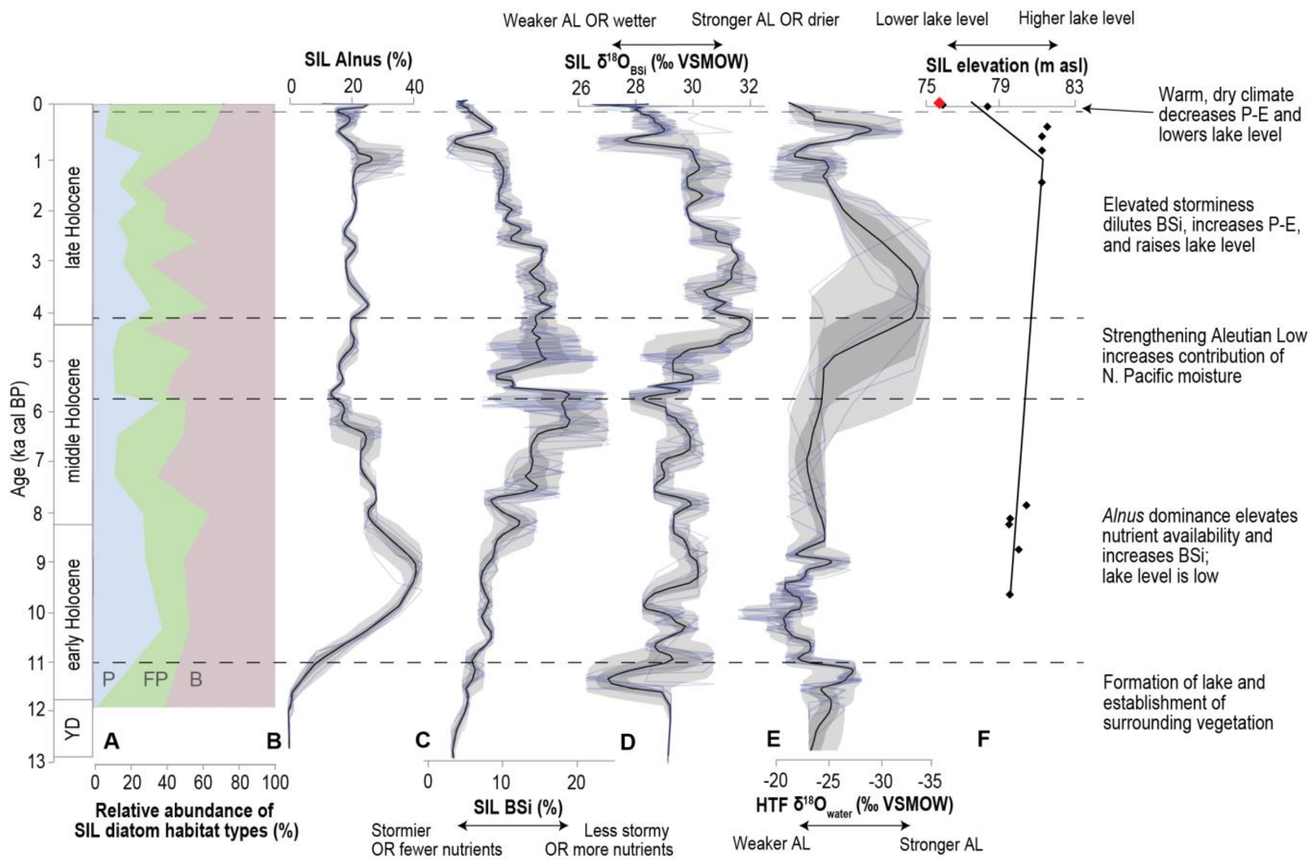

Figure 11: Sunken Island Lake (A) proportions of diatom assemblage habitat types: planktonic (P; blue), facultatively planktonic (FP; green), and benthic (B; purple), (B) relative abundance of *Alnus* (Anderson et al., 2019), (C) biogenic silica (BSi), and (D) $\delta^{18}O_{BSi}$ shown alongside (E) $\delta^{18}O_{water}$ inferred from $\delta^{18}O_{TOM}$ at Horse Trail Fen (note flipped x-axis values) (Jones et al., 2019), and (F) Sunken Island Lake level inferred from dated basal peats in satellite fens and ice shoved ramparts. Black lines in panels B-E are the mean of the age-model ensembles, and dark and light gray shading encompass 68% and 95% of the ensemble members, respectively; blue lines show 5 representative members of the 101-member (SIL) and 55-member (HTF) ensemble. Data plotted using GeoChronR (McKay et al., 2018). Black dots in panel F are radiocarbon ages from satellite fen basal peats and ice-shoved ramparts, and red dot indicates current lake elevation (Table 1). Dashed horizontal lines correspond to important paleoenvironmental events/features, as annotated on the far right.

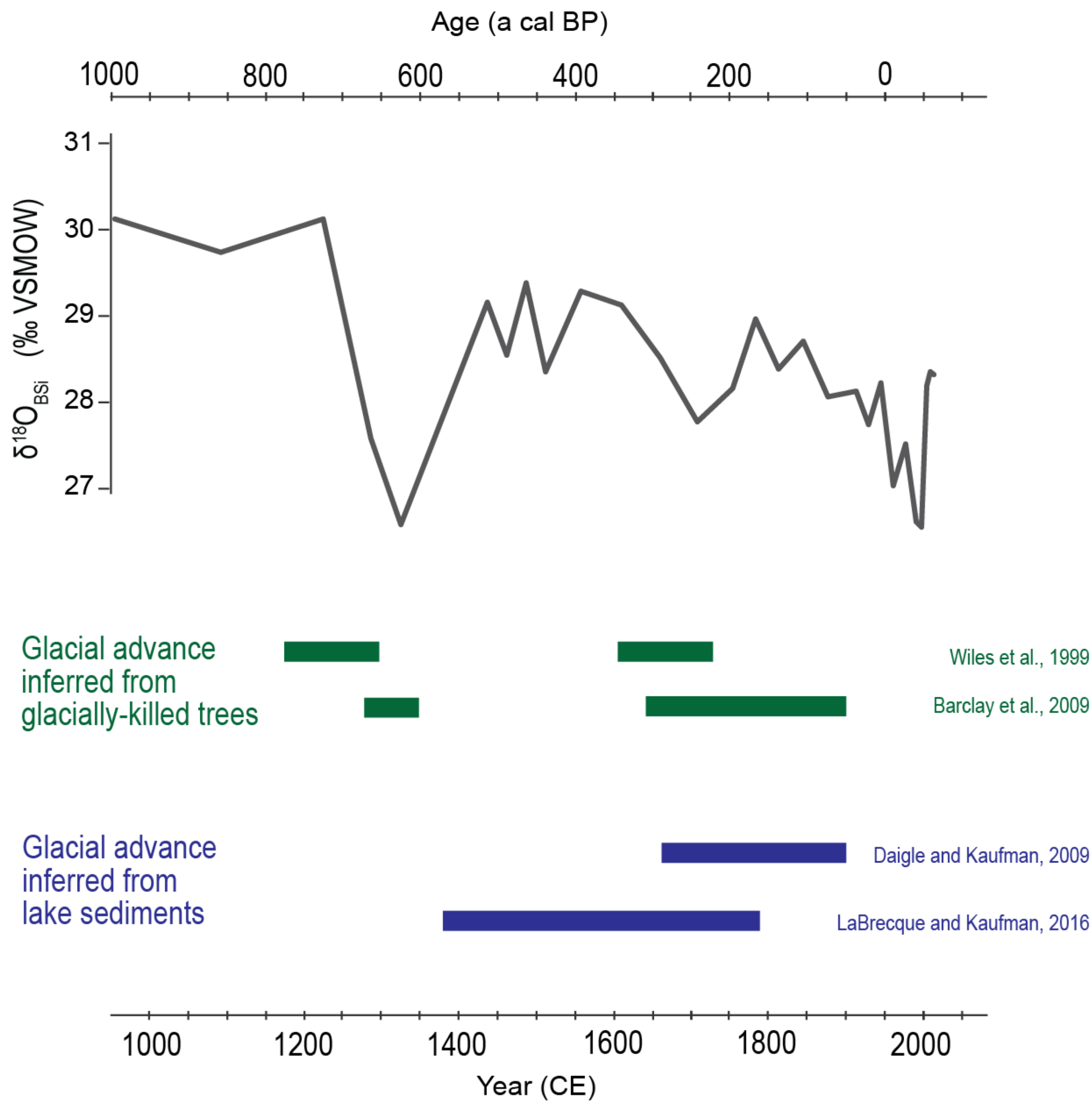

Figure 12: The most recent millennium of the $\delta^{18}O_{BSi}$ from Sunken Island Lake shown alongside inferred glacial advances from sites in the Kenai Mountains and the western Prince William Sound region. Periods of glacial advance are shown as horizontal bars in green for tree-ring records from glacially-killed trees (Barclay et al., 2009; Wiles et al., 1999) and in blue for sediment records from Goat Lake (Daigle and Kaufman, 2009) and Emerald Lake (LaBrecque and Kaufman, 2016).

Core/Site ID	Midpoint depth blf (cm)	^{14}C age (year BP)	Calibrated age (a cal BP)*	Dated material	Lab ID
SIL-04-01	25.1	593 ± 35	603 ± 65	*Alnus* fruit, bryophytes, plant fibers	DAMS009385
SIL-04-01	152.1	2195 ± 15	2249 ± 57	algal copropel	UCIAMS69752
SIL-04-01	207.7	2788 ± 28	2888 ± 69	wood fragments	DAMS009386
SIL-04-01	260.0	3720 ± 20	4042 ± 57	algal copropel, *Betula* fruit	UCIAMS69753
SIL17-1A	382.0	4490 ± 120	5137 ± 290	insect chitin, bryophytes, plant fragments	UCIAMS202769
SIL-04-01	380.0	4915 ± 20	5631 ± 34	plant fragments	UCIAMS34293
SIL-04-01	470.0	4970 ± 230	5718 ± 563	insect chitin, bryophytes	UCIAMS17428
SIL-04-01	519.5	6960 ± 60	7794 ± 114	wood and plant fragments	UCIAMS17579
SIL-04-01	569.0	7000 ± 130	7831 ± 248	insect chitin, bryophytes	UCIAMS17429
SIL-04-01	610.5	7230 ± 110	8060 ± 214	bryophytes, plant fragments	UCIAMS34294
SIL-04-01	631.5	8915 ± 50	10039 ± 172	cladocera chitin	UCIAMS17580
SIL-04-01	656.5	9415 ± 25	10644 ± 68	bryophytes, plant fragments, seeds	UCIAMS69745
SIL-04-01	692.5	10125 ± 20	11771 ± 83	bryophytes	UCIAMS34295
SIL-04-01	705.5	10390 ± 80	12261 ± 280	bryophytes	UCIAMS34296
SIL-04-01	713.5	13460 ± 160	16208 ± 499	insect chitin, aquatic plants	UCIAMS17581
SIL-04-01	720.5	12455 ± 35	14599 ± 335	algal copropel	UCIAMS69755
FEN1B	210.0	7215 ± 25	8014 ± 95	graminoid peat	UCIAMS134786
FEN3	150.0	7860 ± 20	8625 ± 56	graminoid peat	UCIAMS134359
FEN4	180.0	7320 ± 20	8110 ± 69	graminoid-*Drepanocladus* peat	UCIAMS134787
FEN5	210.0	6925 ± 20	7746 ± 67	*Sphagnum*-graminoid peat	UCIAMS134788
FEN6	210.0	8445 ± 20	9479 ± 38	graminoid peat	UCIAMS134789
Wiles	Ice-shoved rampart	350 ± 40	399 ± 91	twig fragments	Beta-245726
102108-1	Ice-shoved rampart	1570 ± 15	1471 ± 55	plant detritus, bark flakes	UCIAMS54689
102108-2	Ice-shoved rampart	630 ± 15	593 ± 50	plant detritus	UCIAMS54690
102108-3	Ice-shoved rampart	920 ± 15	860 ± 60	plant detritus	UCIAMS54691

Table 1: ^{14}C ages for Sunken Island Lake master core, basal ages for satellite fen cores, and ages for ice-shoved ramparts.

*Calibrated age is the median of the calibrated age probability density function. Uncertainty is one half of the two sigma range